Changes in stability ~~and jumps~~ in Dansgaard–Oeschger events: a data analysis aided by the Kramers–Moyal equation

Keno Riechers[1,2*], Leonardo Rydin Gorjão[3,4,5,6,*], Forough Hassanibesheli[7,1], Pedro G. Lind[6,8,9], Dirk Witthaut[3,4], and Niklas Boers[2,1,10]

[1]Research Domain IV – Complexity Science, Potsdam Institute for Climate Impact Research, Telegrafenberg A31, 14473 Potsdam, Germany
[2]Earth System Modelling, School of Engineering & Design, Technical University of Munich, Germany
[3]Forschungszentrum Jülich, Institute for Energy and Climate Research - Systems Analysis and Technology Evaluation (IEK-STE), 52428 Jülich, Germany
[4]Institute for Theoretical Physics, University of Cologne, 50937 Köln, Germany
[5]German Aerospace Center (DLR), Institute of Networked Energy Systems, Oldenburg, Germany
[6]Department of Computer Science, OsloMet – Oslo Metropolitan University, N-0130 Oslo, Norway
[7]Department of Physics, Humboldt-Universität zu Berlin, Newtonstraße 15, 12489 Berlin, Germany
[8]NordSTAR – Nordic Center for Sustainable and Trustworthy AI Research, N-0166 Oslo, Norway
[9]Artificial Intelligence Lab, Oslo Metropolitan University, N-0166 Oslo, Norway
[10]Global Systems Institute and Department of Mathematics, University of Exeter, United Kingdom
[*]These authors contributed equally to this work.

Correspondence: Keno Riechers (keno.riechers@pik-potsdam.de)

Abstract. ~~Dansgaard–Oeschger (DO) events are sudden climatic shifts from cold to substantially milder conditions in the arctic region that occurred during previous glacial intervals. They can be most clearly identified in paleoclimate records of δ^{18}O and dust concentrations from Greenland ice cores, which serve as proxies for temperature and atmospheric circulation patterns, respectively~~During the last glacial interval Northern-Hemisphere climate was punctuated by a series of abrupt changes between two characteristic climate states. The existence of stadial (cold) and interstadial (milder) ~~phases~~ periods is typically attributed to a ~~bistability of~~ hypothesized bistability in the North Atlantic climate system, allowing for rapid transitions from the ~~first to the latter and a more gentle~~ stadial to the interstadial state – the so called Dansgaard–Oeschger (DO) events – and more gradual yet still fairly abrupt reverse ~~shift from the latter to the first. However, the underlying physical mechanisms causing these~~ shifts. The physical mechanisms driving these state transitions remain debated. ~~Here, we conduct a data-driven analysis of the Greenland temperature and atmospheric circulationproxies under the purview of stochastic processes. Based on the Kramers–Moyal equation~~ DO events are characterized by substantial warming over Greenland and a reorganization of the Northern Hemisphere atmospheric circulation, which are evident from concomitant shifts in the δ^{18}O ratios and dust concentration records from Greenland ice cores. Treating the combined δ^{18}O and dust record obtained by the North Greenland ice core project (NGRIP) as a realization of a two-dimensional time-homogeneous and Markovian stochastic process, we present a ~~one-dimensional and two-dimensional derivation of the proxies' drift and diffusion terms, which unravels the features of the climate system's stability landscape. Our results show that: (1) in contrast to common assumptions, the δ^{18}O proxy results from a monostable process, and transitions occur in the record only due to~~ reconstruction of its underlying deterministic drift

based on the leading-order terms of the Kramers–Moyal equation. The analysis reveals two basins of attraction in the ~~coupling to other variables; (2) conditioned on~~ two-dimensional state space that can be identified with the stadial and interstadial states. The drift term of the dust exhibits a double-fold bifurcation structure, while – in contrast to prevailing assumptions – the δ^{18}O component of the drift is clearly monostable. This suggests that the last glacial's Greenland temperatures should not be regarded as an intrinsically bistable climate variable. Instead, the ~~dust concentrations exhibit both mono and bistable states, transitioning between them via a double-fold bifurcation; (3)~~ two-regime nature of the δ^{18}O record is ~~discontinuous in nature, and mathematically requires an interpretation beyond the classical Langevin equation. These findings can help understand candidate mechanisms underlying these archetypal examples of abrupt climate changes.~~

~~In~~ apparently inherited from a coupling to another bistable climate process. In contrast, the bistability evidenced in the dust drift points to the presence of ~~anthropogenically driven climate change, increasing amount of research focuses on the stability of the climate system's current state (Boers, 2021; Heinze et al., 2021; Rosier et al., 2021; Boers and Rypdal, 2021). Several climatic subsystems have been identified to potentially undergo abrupt transitions if global warming exceeds certain thresholds (Lenton and Schellnhuber, 2007; Lenton et al., 2008; Boers et al., 2021). Such abrupt transitions are often conceptually captured~~ two stable circulation regimes of the last glacial's Northern Hemisphere atmosphere.

1 Introduction

Recently, evidence was reported for the destabilisation of climatic subsystems likely caused by continued anthropogenically driven climate change (e.g. Boers et al., 2021; Boers, 2021; Rosier et al., 2021; Boers and Rypdal, 2021). Conceptually, such destabilisation is formulated in terms of ~~dynamical systems transitioning between alternative equilibrium states; for example when a stable equilibrium is lost and a system shifts to another attractor~~ bistable dynamical systems that approach a bifurcation in response to the ~~crossing of a bifurcation point, or when a stochastic perturbation pushes the system from one stable state to another. Furthermore, a system can experience rate-induced transitions during which the system fails~~ gradual change of a control parameter. This setting offers three mechanisms for the system to transition between two alternative stable states (Ashwin et al., 2012): First, the control parameter may cross a bifurcation which dissolves the currently attracting state and necessarily entails a transition to the remaining alternative stable state. Second, random perturbations may push the system across a basin boundary; this is generally more likely the closer the system is to a bifurcation. Third, rapid change of the control parameter may shift the basin boundaries at a rate too high for the system to track the ~~changing domain of attraction of a given equilibrium state and suddenly transitions to another state. Prominent examples for climate elements which~~ moving domain of its current attractor. If global warming – viewed as the control parameter – were to exceed certain thresholds, several elements of the climate system are thought to be at risk ~~of abrupt transitions under sustained anthropogenic greenhouse gas forcing are given by~~ to 'tip' to alternative stable states (Lenton and Schellnhuber, 2007; Lenton et al., 2008; Boers et al., 2021; Armstrong McKay et al., 202 , among them the Greenland Ice Sheet ~~(Boers, 2021)~~(Boers and Rypdal, 2021), the Amazon rainforest ~~(?)~~(Boulton et al., 2022) , the Atlantic Meridional Overturning Circulation (AMOC) ~~(Boulton et al., 2014; Boers and Rypdal, 2021)~~(Boulton et al., 2014; Boers, 202 , and the West Antarctic ice sheet (Rosier et al., 2021).

While the conceptual understanding of abrupt transitions in terms of dynamical system theory is well established, the only observational evidenceof abrupt climate transitions stems The possibility of alternative stable states of the entire climate system or its subsystems (and transitions between these) has been discussed at least since the 1960s (e.g. Ghil, 1975; North, 1975; Stommel, 1961) . Empirical evidence, however, that the climate system or its subsystems can indeed abruptly transition between alternative equilibria is available only from proxy records that encode the evolution of past climate variability (Brovkin et al., 2021). Understanding the physical causes of such past which allow to reconstruct past climate states prior to the instrumental period (e.g. Brovkin et al., 2021; Boers et al., 2022, and references therein). Given that comprehensive Earth system models continue to have problems in simulating abrupt climate changes is crucial for improving the capability of comprehensive Earth System Models to faithfully simulate such transitions, and is therefore a prerequisite and especially in reproducing abrupt changes evidenced in proxy records (Valdes, 2011), studying abrupt changes recorded by paleoclimate proxies is key for gaining a better understanding of the physical mechanisms involved and for assessing the risk of abrupt climate changes under future warming scenarios (Valdes, 2011; Boers et al., 2021). The most prominent example of past abrupt climate shifts are risks of future abrupt transitions.

In this context, our study investigates the Dansgaard–Oeschger events – (DO) events; a series of sudden warming events that dominated Greenland temperatures throughout the last glacial cycle, e.g., Refs. (Johnsen et al., 1992; Dansgaard et al., 1993; North Greenla . These events have first been revealed in δ^{18}O record abrupt warming events over Greenland first evidenced in stable water isotope records from Greenland ice cores (see Fig. 1), which serve as proxies for past air temperatures at the drilling site (Jouzel et al., 1997; . Taking place on time scales of decades, the amplitudes of warming (Dansgaard et al., 1982, 1984, 1993; Johnsen et al., 1992; North Green . While locally the temperature increases are estimated to exceed 10°C in most cases, and reach up to be as large as 16°C in the annual mean temperature over Greenland (Steffensen et al., 2008; Kindler et al., 2014; Gkinis et al., 2014; Capron et al., 2021) . The sudden temperature increase is usually followed by a phase of moderate cooling, before the temperatures ultimately relax back to their pre-event levels in a second phase of more abrupt cooling. While the duration of the relatively warm phases termed Greenland Interstadials (GIs) stretches from centuries to millennia, the cold Greenland Stadials (GSs) typically persists over millennia before another sudden warming event starts a new DO cycle (Rasmussen et al., 2014). Moreover, in addition to δ^{18}O, further Greenland ice core proxies bear the signature of (Kindler et al., 2014), a (weaker) signature of these events can be found in numerous records across the globe (e.g. Voelker, 2002; Menviel et al., 2020, and references therein), indicating changes in other climatic subsystems such as Antarctic average temperatures (e.g. WAIS Divide Project Members, 2015; EPICA Community Member , the DO cycles, such as dust (Fuhrer et al., 1999; North Greenland Ice Core Projects members, 2004) and sodium concentrations (Erhardt e , or the thickness of the annual deposition layers (Erhardt et al., 2019). The common interpretation of these concomitant Asian and South American Monsoon system (e.g. Wang et al., 2001; Kanner et al., 2012; Cheng et al., 2013; Li et al., 2017; Corrick et al., 2020) or the Atlantic meridional overturning circulation (AMOC) (e.g. Lynch-Stieglitz, 2017; Henry et al., 2016; Gottschalk et al., 2015) . The global puzzle of more or less abrupt shifts in the different proxy time series is that the sudden Greenland warming events were accompanied by sudden synchrony (within the limits of dating uncertainties) with DO events found in versatile paleoclimate proxy records points to a complex scheme of interactions between climatic subsystems involved in the DO variability that dominated the last glacial period. While multiple lines of evidence indicate a central role of changes in

the ~~atmospheric circulation, retreat of the North Atlantic and Nordic Sea's sea ice cover, and increases in the amount of local precipitation, respectively, e.g., Refs. (Li and Born, 2019; Erhardt et al., 2019; Menviel et al., 2020). Importantly, despite substantial progress in recent years, no general consensus has yet been achieved regarding the mechanism that causes the DO events. Different patterns of interaction between the AMOC, sea ice cover, the Northern Hemisphere atmospheric circulation, and even the continental ice sheets have been proposed and explored to explain the emergence of DO cycles (Broecker et al., 1985; Li et al., .~~ overturning strength of the AMOC (e.g. Lynch-Stieglitz, 2017; Menviel et al., 2020), to date there is no consensus about the ultimate trigger of DO events.

~~Here, in order to reconstruct the dynamics that governed Greenland temperatures during the last glacial, we assume an inverse modelling approach, in a fashion similar to the analysis conducted in, e.g., Refs. (Ditlevsen, 1999; Livina et al., 2010; Kwasniok, 2013; Kru . The key concept is to regard the paleo-climate~~ An important branch of research has assessed the performance of low-dimensional conceptual models in explaining the DO variability of the Greenland ice core records (e.g. Ditlevsen, 1999; Livina et al., 2010; Kwasniok, 2 . Typically, one-dimensional multi- or bistable models (Ditlevsen, 1999; Livina et al., 2010; Kwasniok, 2013; Lohmann and Ditlevsen, 201 or two-dimensional relaxation oscillators (Kwasniok, 2013; Mitsui and Crucifix, 2017; Roberts and Saha, 2017; Lohmann and Ditlevsen, 2 have been invoked, forced by either slowly changing climate background variables such as CO_2 or changing orbital parameters, by noise or by both. To the best of our knowledge, to date Boers et al. (2017) presented the only inverse-modelling approach to simulate a two-dimensional Greenland ice core proxy record – δ^{18}O and dust – with regards to its DO variability. Likewise in two dimensions, we present here a data-driven investigation of the couplings between Greenland temperatures and the larger scale Northern hemisphere state of the atmosphere represented by the NGRIP δ^{18}O ratio and dust concentration records (North Greenland Ice Core Projects members, 2004; Gkinis et al., 2014; Ruth et al., 2003). Treating the combined δ^{18}O and dust record as the realisation of a ~~Markovian and stationary stochastic process (Kondrashov et al., 2005, 2015)which can be described in terms of a stochastic differential equation. In this setting there exist different ways to estimate the deterministic drift and the stochastic diffusion component. Drawing on~~ time-homogeneous Markovian stochastic process (Kondrashov et al., 2005, 2015) , we reconstruct the corresponding deterministic two-dimensional drift using the Kramers–Moyal equation ~~(~~Kramers, 1940; Moyal, 1949; Tabar, 2019) ~~, we recover the underlying drift term – or the potential landscape – that discloses the stability configuration of the system, together with the diffusion term.In particular, we present the first Kramers–Moyal-based reconstruction~~ and reveal evidence for bistability of the coupled δ^{18}O-dust 'system'. Compared to the previously mentioned studies, this approach has the advantage that the estimation of the drift is non-parametric, i.e. it assumes no *a priori* functional structure for the drift, and that it assesses the stability configuration of the two-dimensional ~~drift in the coupled system comprised of Greenland ice core~~ record as opposed to the numerous studies concerned with one-dimensional proxy records.

In the state space spanned by δ^{18}O ~~values~~ ratios and dust concentrations~~. The Kramers–Moyal equation generalises the Fokker–Planck description of stochastic processes, including explicitly the presence of discontinuous elements. In this sense, it steps outside the classical description of a Langevin process, yet preserves a similar interpretation of the drift and diffusion of~~ , based on our results we identify two regions of convergence concentrated around two stable fixed points, which can be associated with Greenland stadials and interstadials. We show that the global bistability is rooted in the dust component of the drift, exhibiting what seems to be a double-fold bifurcation parameterised by δ^{18}O. This asserts a genuine bistability to

the glacial Northern-Hemisphere atmosphere. In contrast, the ~~processes~~δ^{18}O drift component is monostable across all dust values, suggesting that the two regimes evidenced in past Greenland temperature reconstructions are not the signature of intrinsic bistability but that of coupling another bistable subsystem, which – according to our results – may be the atmospheric large-scale circulation.

This article is structured as follows: ~~In Sec. 2 we introduce the paleo-climatic proxies under examination and the detrending method used to ensure that the data is approximately stationary. In Sec. 3~~ We first present the paleoclimate proxies analysed in this study and explain how we pre-processed the data to make it suitable for estimating Kramers-Moyal coefficients (Sect. 2). Subsequently, we introduce the two-dimensional Kramers–Moyal ~~expansion as the prime method to extract the potential landscape and examine the influence of stochastic noise and possible discontinuous elements within the records.In Sec. 4 we present the results, beginning with a one-dimensional analysis of the two proxies, in Sec. **??**. We examine their separate potential landscapes and higher-order Kramers–Moyal coefficients, and therein manifest the need to augment our examination to a~~ equation which is key for the analysis (Sect. 3). Section 4 provides the reconstruction of the two-dimensional ~~plane. This is consequently discussed in Sec. **??**, where we uncover the conditioned potential landscapes of the joint proxy process. We examine the stability configurations of the δ^{18}O and dust time series in respective comparison, unveiling the arguments for mono-stability of the δ^{18}O, and a mixed set of states for the dust, which undergoes an double-fold bifurcation parametrised by the δ^{18}O. In Sec~~drift, and Sect. 5 discusses the results and how they relate to previous studies. In the final Sect. 6 we ~~discuss the results and consequences of our findings in a paleoclimate context~~summarise our main findings and detail the research questions that follow from these.

2 Data and pre-processing

The analysis presented here is based primarily on the joint δ^{18}O ratio and dust concentration time series obtained by the North Greenland Ice Core Project (NGRIP) ~~(Ruth et al., 2003; North Greenland Ice Core Projects members, 2004; Gkinis et al., 2014) . The concentration~~ (North Greenland Ice Core Projects members, 2004; Ruth et al., 2003; Gkinis et al., 2014). From 1404.75 m to 2426.00 m of depth in the NGRIP ice core, data are available for both proxies at a spatially equidistant resolution of 5 cm. This translates into non-equidistant temporal resolution ranging from sub-annual resolution at the beginning to $\sim$ 5 years at the end of the period 59944.5 – 10276.4 yr b2k. Lower resolution data (20-year means) (Rasmussen et al., 2014; Seierstad et al., 2014) reaching back to the last interglacial period (see Fig. 1) are only used for illustrative purpose but not for the analysis. All ages are according to the Greenland Ice Core Chronology 2005 (GICC05), the common age-depth model for both proxies (Vinther et al., 2006; Rasm

The ratio of stable water isotopes, expressed as δ^{18}O values in units of permil, is a proxy for the site temperature at the time of precipitation ~~(Jouzel et al., 1997; Gkinis et al., 2014).~~ and hence the abrupt shifts present in the data qualitatively indicate the abrupt warming events over Greenland (Jouzel et al., 1997; Johnsen et al., 2001).

The concentration of dust, i.e. the number of particles with diameter above one micron per millilitre, is commonly interpreted as a proxy for the state of the hemispheric atmospheric circulation (e.g. Fischer et al., 2007; Ruth et al., 2007; Schüpbach et al., 2018; Erhar

. More specifically, it is assumed to be controlled mostly by ~~two factors~~three factors (Fischer et al., 2007): First, by climatic conditions at the emission source, ~~that is,~~ i.e. the dust storm activity over East Asian deserts preconditioned on generally dry regional climate~~. Second, ~~; second, by the transport efficiency, which is affected by the strength and position of the polar jet stream ~~(Ruth et al., 2007; Schüpbach et al., 2018; Erhardt et al., 2019)~~; and third, the depositional process which is mostly determined by local precipitation patterns. Correspondingly, the substantial changes in the dust concentrations across DO events are interpreted as large-scale reorganisations of the Northern Hemisphere's atmospheric circulation ~~(Erhardt et al., 2019)~~ . Typically, atmospheric changes affecting the dust flux onto the Greenland ice sheet are accompanied by changes in the snow accumulation of opposite sign (e.g. Fischer et al., 2007). This enhances the corresponding change of the recorded dust particle concentration. However, for high-accumulation Greenland ice cores – such as NGRIP – the dust concentration changes still serve as a reliable indicator of atmospheric changes according to Fischer et al. (2007). Since the dust concentrations approximately follow an exponential distribution, we consider ~~in the following re-scaled values by taking the natural logarithm and multiplying by −1~~ the negative natural logarithm of the dust concentration in order to emphasise the similarity to the δ^{18}O time series~~(cf. Fig. 1)~~. For ease of notation~~we will~~ , we will always use the term dust (or dust concentrations) although technically we refer ~~to the~~ its negative natural logarithm~~of the dust concentration~~.

~~Data is available for both proxies at an equidistant resolution of 5 cm, from 1346.45 m to 2426.00 m of depth in the NGRIP ice core. This translates into non-equidistant temporal resolution ranging from sub-annual resolution at the beginning to ∼ 5 years at the end of the period 9527.3 – 59944.5 yr b2k (before the year 2000). All ages are according to the Greenland Ice Core Chronology 2005 (GICC05), the common age-depth model for both proxies (Vinther et al., 2006; Rasmussen et al., 2006; Andersen et al., 2~~

In Fig. 1 we show the original low-resolution (b and c) and the pre-processed high-resolution data (f and g) together with corresponding histograms (h), also given in Fig. 3(a). Clearly, two regimes can be visually distinguished: Greenland stadials are characterised by low δ^{18}O ratios and high dust concentrations. Greenland interstadials (grey shading in panels (f) and (g) of Fig. 1) in general exhibit the reversed configuration besides a mild trend toward stadial conditions, which can be more or less pronounced during the individual interstadials. In our study, we use the categorisation of the climatic periods as presented by Rasmussen et al. (2014). The two-regime character of the time series translates into a bimodal histogram of the dust data, as seen in Fig. 1 (h). In the case of the δ^{18}O data, the stronger trend during interstadials and the higher relative noise amplitude masks a potential bi-modality and the histogram appears unimodal.

The analysis conducted in this work ~~assumes stationarity of the underlying~~ relies on the following assumptions and technical conditions:

(i) the data-generating process ~~. However, Boers *et al.* (Boers, 2018) pointed out~~ is sufficiently time-homogeneous over the considered time period;

(ii) the process is Markovian at the sampled temporal resolution;

(iii) the data is equidistant in time;

(iv) the relevant region of the state space is sampled sufficiently densely by the available data.

With regard to (i) a low-frequency influence of the background climate ~~, for example, expressed in terms of global ice volume,~~ on the proxy values and on the frequency of DO events ~~, whith~~ is evident (see Fig. 1), with suppressed DO variability during the coldest parts of the glacial ~~such as the Last Glacial Maximum. We therefore complement the NGRIP dust and δ^{18}O data with a reconstruction of the global average surface temperature as presented in Ref. (Snyder, 2016). Moreover, Boers *et al.* (Boers et al., 2017) highlighted that δ^{18}O and dust show high co-variability over the period 59–22 kyr b2k. However, this relationship weakens after 22 kyr b2k, thus constraining the potential data segment eligible for our study. Excluding also the Last Glacial Maximum from the data, we~~ and longer interstadials for its warmer parts (e.g. Rial and Saha, 2011; Roberts and Saha, 2017; M . We therefore restrict our analysis to the period 59–27 kyr b2k, which is characterised by a fairly stable background climate and persistent co-variability between dust and δ^{18}O~~. To compensate for~~ (Boers et al., 2017). To remove the remaining influence of the background climate on the climate proxy records ~~,~~ we remove a ~~linear trend with respect to the global average surface temperature~~ trend that is nonlinear in time from both time series~~(see App. ?? for the details).After the detrending we consider the data as the outcome of an approximately stationary process. As the final step of the pre-processing the data is binned to temporally equidistant increments of 5 years and normalised with respect to the average amplitude of the DO transitions.~~

~~Lastly, the analysis in this work is based on Markovian stochastic processes. To assess whether the data is Markovian, we analyse the auto-covariance function of the increments of the detrended data . The covariance is largely zero everywhere, except for a weak anti-correlation at the shortest lag, supporting the assumption that the data is approximately Markovian (see App. ??)~~ .

3 ~~Methods~~

~~In this section, we present the methods used to study the coupled δ^{18}O and dust dynamics, drawing on the theory of stochastic processes and stochastic differential equations. Starting from the well-known Langevin process, we introduce the broader Kramers–Moyal (KM) framework. The Fokker–Planck equation associated with a Langevin process will be expanded to the more general Kramers–Moyal equation in one and two dimensions. While the KM setting is suited for the treatment of complex noise, the interpretation of a deterministic drift component is preserved. This allows us to investigate the stability configuration of the coupled δ^{18}O–dust system. We begin by shortly introducing one-dimensional stationary Markovian stochastic processes.~~

2.1 ~~Continuous and discontinuous stochastic processes~~

~~A one-dimensional stochastic process is a mapping from time $t \in \mathbb{R}$ into some adequate state space that describes the dynamics of a random variable $x(t)$, subject to random fluctuations. A prominent example for a stochastic process is given by the stationary Langevin equation, a stochastic differential equation of the form~~ This trend is obtained by linearly regressing the proxy data against reconstructed global average surface temperatures (Snyder, 2016); Fig. 1 illustrates the detrending scheme: Due to the two-regime nature of the time series, a simple linear regression of the proxy variables onto the global average surface temperatures would overestimate the temperature dependencies. Instead, we separate the data from Greenland stadials

and Greenland interstadials and then minimise the quantity

$$R = \left(\sum_{i=1}^{N} x(t_i) - a\Delta T(t_i) - \begin{cases} b_{\mathrm{GI}}, \text{ if } t_i \in \mathrm{GI} \\ b_{\mathrm{GS}}, \text{ if } t_i \in \mathrm{GS} \end{cases} \right)^2 \tag{1}$$

once for $x = \delta^{18}\mathrm{O}$ and once for x taken as dust concentrations. Each optimisation yields individual optimal values for the parameters a, b_{GI}, and b_{GS} (See Fig. 1 panels (d) and (e) for $\delta^{18}\mathrm{O}$ and dust concentration, respectively). For a given time t_i we write $t_i \in$ GS (GI) to indicate that t_i falls into a stadial (interstadial) period. The index i runs over all data points and N denotes the total number of data points. The resulting slope a is used to detrend the original data with respect to the time dependent background temperature:

$$\mathrm{d}x_{\mathrm{detrended}}(t_i) = a(x)\mathrm{d}t + b(x t_i)\mathrm{d}B - a\Delta T(t_i), \tag{2}$$

~~with the drift term $a(x)$, the diffusion term $b(x)$, and an uncorrelated Brownian motion $B(t)$. If the properties of the dynamics do not change over time, i.e. $a(x)$ and $b(x)$ do not depend on time, these processes are called *stationary*. While the Langevin equation is continuous in time, stochastic processes can in principle have discontinuous features, such as sudden jumps. An easy way to incorporate discontinuities is to include in Eq. (??) an elementary Lévy process $L(t)$, modulated with an amplitude $h(x)$ (Applebaum, 2011)~~

$$\mathrm{d}x(t) = a(x)\mathrm{d}t + b(x)\mathrm{d}B(t) + h(x)\mathrm{d}L(t).$$

~~The interpretation of $a(x)$ and $b(x)$ as drift and diffusion remains preserved under this generalisation. Note that Langevin processes are just a subclass of Lévy processes, and all these processes are Markovian.~~

2.1 ~~The one-dimensional Kramers–Moyal equation~~

~~Stochastic processes can be either described in terms of random variables, following a stochastic differential equation as introduced above, or in terms of the evolution of their conditional probability density function $p(x,t|x',t')$, following a partial differential equation. If a single particle's motion is governed by the Langevin equation, its probability density function $p(x,t|x',t')$ evolves according to the Fokker–Planck equation, given by Fokker (1913, 1914); Planck (1917)~~

$$\frac{\partial}{\partial t}p(x,t|x',t') = -\frac{\partial}{\partial x}D_1(x)p(x,t|x',t') + \frac{\partial^2}{\partial x^2}D_2(x)p(x,t|x',t'),$$

~~which we consider in a stationary case as above, i.e.without explicit time dependence of the coefficients $D_1(x)$ and $D_2(x)$. These coefficients directly relate to the drift and diffusion terms given in Eq. (??) by~~

$$D_1(x) = a(x),$$

$$D_2(x) = \tfrac{1}{2}b^2(x).$$

The Fokker–Planck equation can only describe continuous processes (Risken and Frank, 1996; Stemler et al., 2007; Gardiner, 2009; Tab . Giving up the condition of continuity, the temporal evolution of the conditional probability density follows the Kramers–Moyal equation Kramers (1940); Moyal (1949); van Kampen (1961)

$$\frac{\partial}{\partial t}p(x,t|x',t') = \sum_{m=1}^{\infty}\left(-\frac{\partial}{\partial x}\right)^m D_m(x)\,p(x,t|x',t'),$$

where $D_m(x)$ denotes the mth Kramers–Moyal (KM) coefficient, defined from the corresponding conditional moments $M_m(x,\tau)$ of the variable x and a time-lag τ, i.e.

$$\begin{aligned} D_m(x) &= \frac{1}{m!}\lim_{\tau\to 0}\frac{M_m(x,\tau)}{\tau} \\ &= \frac{1}{m!}\lim_{\tau\to 0}\frac{1}{\tau}\langle (x(t+\tau)-x(t))^m\,|_{x(t)=x}\rangle\,, \end{aligned}$$

where $\langle\cdots\rangle$ denotes the expected value . If a stochastic process is 'sufficiently' continuous, the third and all higher KM coefficients vanish according to Pawula's theorem (Pawula, 1967a, b), and Subsequently, the Kramers–Moyal equation (Eq. (**??**)) reduces to the simpler Fokker–Planck (Fokker–Planck–Kolmogorov) equation (Eq. (**??**)) . While the Langevin equation is the direct counterpart of the Fokker–Planck equation, for the Kramers–Moyal equation a single particle's equation of motion can assume different functional forms that describe different (discontinuous) stochastic processes (one example is given by Eq. (**??**)) . However, for numerous of these stochastic processes, the KM coefficients can be related to detrended data are normalised by subtracting their respective means and dividing by their respective standard deviations. After the detrending, all stadial (resp. interstadial) periods exhibit almost the same level of values, which allows considering the data as the outcome of a time-homogeneous and stationary process (compare Fig. 1 panels (f) and (g)). Levelling out the differences between the recurring climate periods guarantees a sufficiently dense sampling of the properties of the stochastic process in the spirit of Eq. (**??**). Importantly, interpretation of the first and second KM coefficients as the drift and diffusion terms, respectively, is preserved in the presence of discontinuities. relevant region of the state space (iv) and prevents a blurring of the drift reconstruction (i).

In practice, as can be understood from Eq. (**??**), one of the pivotal elements of using a description such as the Kramers–Moyal equation is the possibility to estimate the coefficients $D_m(x)$ directly from data. To retrieve the KM coefficients $D_m(x)$ from a single realisation of a stochastic process Stationarity tests provide further confirmation that the detrended data can be regarded as stationary: We have applied two separate tests to assess the stationarity of the detrended data on time scales beyond single DO cycles. These tests are the Augmented Dickey–Fuller test (ADF) and the Augmented Dickey–Fuller-GLS test (ADF-GLS). Both tests test the possibility of a unit-root in the time series (null hypothesis). The alternative hypothesis is that the time series does not have a unit root, i.e.a single time series, we evaluate the transition probability densities in the limit of a vanishing time step $\tau \to 0$, which numerically corresponds to considering the shortest increment Δt in the data ($\tau \to \Delta t$). In other words

$$D_m(x) \approx \frac{1}{m!}\frac{1}{\Delta t}\langle (x(t+\Delta t)-x(t))^m\,|_{x(t)=x}\rangle\,,$$

			dust	δ^{18}O
		critical value	statistics (p-value) [lag]	statistics (p-value) [lag]
ADF	no trend	-1.9410	-5.0519 (8.362e-07) [6]	-6.8037 (1.661e-10) [15]
	no constant	-2.8620	-5.0515 (1.753e-05) [6]	-6.8034 (2.208e-09) [15]
	constant and linear trend	-3.4112	-5.3732 (4.082e-05) [5]	-7.3196 (2.644e-09) [15]
	constant, linear, and quadratic trends	-3.8333	-5.4810 (1.382e-04) [5]	-7.5415 (4.278e-09) [15]
ADF-GLS	constant	-1.9470	-3.4422 (6.373e-04) [6]	-3.7747 (1.904e-04) [15]
	constant and linear trend	2.8499	-5.2217 (9.989e-06) [5]	-6.6558 (1.487e-08) [15]

Table 1. Unit root test of the detrended data. ADF refers to the Augmented Dickey–Fuller test; ADF-GLS refers to the Augmented Dickey–Fuller-GLS test. We reject the presence of a unit-root in each of the time series at $p < 0.05$.

~~with which we estimate the various KM coefficients directly from the data. Details on the numerical implementation of this~~
~~estimation procedure are given in App. A and App. **??**~~, it is stationary. We can safely reject the presence of a unit root in each time series at $p < 0.05$ (see Tab. 1).

~~An important remark which will help in the following analysis of the paleoclimate time series is~~ There is a trade-off between the conditions (i) and (iv) concerning the choice of the data window. While an even shorter window would assure time-homogeneity of the ~~physical interpretation of the drift. Thinking of the stochastic variable $x(t)$ as the position of a point particle allows to interpret the integral over the drift as a potential landscape~~

~~$$V(x) = -\int_{-\infty}^{x} D_1(x')\,\mathrm{d}x' + c.$$~~

dynamics with higher confidence, the sampling of the state space would become insufficiently sparse. The above choice (59–27 kyr b2k) guarantees sufficiently many recurrences of the pre-processed two-dimensional trajectory to the relevant state space regions to perform statistical analysis. To obtain a time-equidistant records (iii), the data are binned to temporally equidistant increments of 5 years. ~~This potential controls the motion of the particle in the sense that the deterministic part of the dynamics will drive the particle to the bottom of potential wells. Stochastic fluctuations, however, may counteract this relaxation and push the particle out of equilibrium and even into another well. We will use this to best illustrate the stability configuration of each proxy.~~

2.1 ~~Distinguishing between continuous and discontinuous processes in time series~~

~~The striking difference between the Fokker–Planck equation (**??**) and the Kramers–Moyal equation (**??**) is the presence of higher-order Kramers–Moyal coefficients $D_m(x), m > 2$, which arise as the direct consequence of discontinuities in a Markovian stochastic process.~~

~~Consider the KM coefficients $D_m(x)$ estimated from the records of a stochastic process as outlined above. A first metric to discern whether this process is discontinuous is to evaluate the ratio of the fourth KM coefficient to the second one ,~~

~~$D_4(x)/D_2(x)$. This roughly compares the size of the the discontinuous paths with the size of the diffusive effects . Thus, values of the ratio $D_4(x)/D_2(x)$ close to zero imply continuous sample paths with no jumps in the data. Values larger than zero, i.e. ~ 1, indicate that the jump contribution is of the same order of magnitude as the diffusive contribution (Risken and Frank, 1996; Anvari et al~~

The question of Markovianity (ii) is the most difficult to answer unambiguously. Here we draw on the following heuristic argument: The autocorrelation functions of the increments of both proxies shown in Fig. 2 exhibit weak anti-correlation at a shift of one time step and exhibit negligible correlations beyond this. Such small level of correlation certainly speaks against memory effects to have played a major role in the emergence of the given time series and hence in favour of considering the data Markovian.

~~This assessment can be refined by regarding the Lehnertz–Tabar Q-ratio (Lehnertz et al., 2018), which takes advantage of~~ Finally, the fact that ~~continuous and discontinuous systems 'scale' in a different fashion. While a purely continuous stochastic process diffuses proportionally to time t (or possibly a power of time t^β in anomalous diffusions (Einstein, 1905; von Smoluchowski, 1906;) , discontinuous processes can cover large distances in short times, i.e. jump, which causes them to exhibit no scaling relations with time t. This can be evaluated via the comparative convergence of the conditional moments $M_m(x,\tau)$ of a stochastic process with the scaling τ (cf. Eq. (??)), given by~~ the NGRIP record exhibits an exceptionally high resolution (iv) compared to other paleoclimate archives and that the two time series share the same time axis are further preconditions for our endeavor.

3 Methods

In this work, we treat the combined δ^{18}O and dust record as a two-dimensional, time-homogeneous Markovian stochastic process of the form

$$Q\mathrm{d}\boldsymbol{x}=\boldsymbol{F}(x,\tau\boldsymbol{x})=\frac{M_6(x,\tau)}{5M_4(x,\tau)}\sim\mathrm{d}t+\mathrm{d}\boldsymbol{\xi}, \tag{3}$$

where ~~the moments $M_m(x,\tau)$ are given by Eq. (??). If the process is purely diffusive $Q(x,\tau)\sim\tau$ (~~$\boldsymbol{\xi}$ denotes a general δ-correlated driving noise. It may be state-dependent – i.e.~~a linear function of τ) and if the process yields discontinuous trajectories $Q(x,\tau)\sim k$ (i.e. a constant over τ).~~

3.1 ~~The two-dimensional case~~

~~Above, we have introduced the Kramers–Moyal equation for a one-dimensional stochastic process. However, with δ^{18}O and dust representing two different yet coupled climate proxy variables, it is necessary to analyse their records in a combined manner. The~~ , explicitly depend on $\boldsymbol{x}$ – and contain discontinuous elements. No further specification is needed for the analysis presented here. The reconstruction of the two-dimensional drift $\boldsymbol{F}(\boldsymbol{x})$ is based on the Kramers–Moyal ~~equation is given~~

by (Risken and Frank, 1996; Lind et al., 2005; Tabar, 2019; Rydin Gorjão et al., 2019) (KM) equation, which reads

$$\frac{\partial}{\partial t}p(x_1,x_2,t|x_1',x_2',t') = \sum_{i,j=1}^{\infty}(-1)^{i+j}\left(\frac{\partial^{i+j}}{\partial x_1^i \partial x_2^j}\right)D_{i,j}(x_1,x_2)p(x_1,x_2,t|x_1',x_2',t').$$

$$\frac{\partial}{\partial t}p(x_1,x_2,t|x_1',x_2',t') = \sum_{i,j=1}^{\infty}(-1)^{i+j}\left(\frac{\partial^{i+j}}{\partial x_1^i \partial x_2^j}\right)D_{i,j}(x_1,x_2)p(x_1,x_2,t|x_1',x_2',t') \tag{4}$$

The in two dimensions, where $p(x_1,x_2,t|x_1',x_2',t')$ denotes the probability for the system to assume the state (x_1,x_2) at time t, given that it was in the state (x_1',x_2') at the time t'. The coefficients $D_{i,j}(x_1,x_2)$ of the two-dimensional Kramers–Moyal equation can be estimated – analogously to the one-dimensional coefficients as explained in Tabar (2019) – from the record a realisation of a two-dimensional stochastic process ~~$\boldsymbol{x}(t) = (x_1(t),x_2(t))$.~~

The drift $\boldsymbol{x}(t) = (x_1(t),x_2(t))$. The terms $D_{1,0}(\boldsymbol{x})$ and $D_{0,1}(\boldsymbol{x})$ carry the same meaning as before. However, relating the higher order two-dimensional KM coefficients to combine to the deterministic drift that governs the stochastic process:

$$\boldsymbol{F}(x_1,x_2) = (D_{1,0}(x_1,x_2),D_{0,1}(x_1,x_2))^\top. \tag{5}$$

In this work we only consider the first-order KM coefficients which allow us to uncover the deterministic non-linear features behind the stochastic data. In principle, for a given stochastic process model, the various parameters of a stochastic differential equation higher-order KM coefficients can be used to estimate the corresponding noise parameters (see e.g. Anvari et al., 2016; Lehnertz et . However, this is not straightforward . In a two-dimensional setting, we can still use $D_{1,0}(\boldsymbol{x})$ and $D_{0,1}(\boldsymbol{x})$ to similarly investigate the deterministic part of the underlying dynamics in state space. An intuitive way to understand the motion of a two-dimensional process is to examine the vector field generated by the two drifts, given by in two dimensions and we deliberately refrain from an up-front selection of a process model in this work. Furthermore, a reliable estimate of higher order coefficients in two dimensions is prevented by insufficient data density. A general derivation of the Kramers–Moyal equation can be found in (Kramers, 1940; Moyal, 1949; Risken and Frank, 1996; Gardiner, 2009; Tabar, 2019).

In practice, in order to carry out the estimation of the first-order KM coefficients as defined in Eq. (4) we map each data point in the corresponding state space to a kernel density and then take a weighted average over all data points:

$$\begin{aligned} D_{1,0}(\boldsymbol{x}) &\sim \frac{1}{n!}\frac{1}{m!}\frac{1}{\Delta t}\langle(x(t+\Delta t)-x(t))|\boldsymbol{x}(t)=\boldsymbol{x}\rangle \\ &\sim \frac{1}{m!}\frac{1}{\Delta t}\frac{1}{N}\sum_{i=1}^{N-1}K(\boldsymbol{x}-\boldsymbol{x}_i)(x_{i+1}-x_i) \end{aligned} \tag{6}$$

$(x_1,x_2) = D_{1,0}(x_1,x_2),D_{0,1}(x_1,x_2)^\top.$

$$D_{0,1}(\boldsymbol{x}) \sim \frac{1}{n!}\frac{1}{m!}\frac{1}{\Delta t}\langle (y(t+\Delta t)-y(t))|\boldsymbol{x}(t)=\boldsymbol{x}\rangle \\ \sim \frac{1}{n!}\frac{1}{m!}\frac{1}{\Delta t}\frac{1}{N}\sum_{i=1}^{N-1} K(\boldsymbol{x}-\boldsymbol{x}_i)(y_{i+1}-y_i), \tag{7}$$

~~For various applications where the fluctuations are not comparable in size, i.e. where the diffusion elements are not of similar scale, one can draw a clearer picture of the motion of the two-dimensional system by referring to an *effective* vector field~~ with $\boldsymbol{x}=(x,y)^\top$, and $m!$ and $n!$ either $0!$ or $1!$, depending.

Alike selecting the number of bins in a histogram, when employing kernel-density estimation with a Nadaraya–Watson estimator for the Kramers–Moyal coefficients $D_{m,n}(\boldsymbol{x})$, one needs to select both a kernel and a bandwidth (Nadaraya, 1964; Watson, 1964; . Firstly, the choice of the kernel is the choice of a function $K(\boldsymbol{x})$ for the estimator $\widehat{f}_h(\boldsymbol{x})$, where h is the bandwidth at a point $\boldsymbol{x}$

$$\widehat{f}_h(x_1,x_2\boldsymbol{x}) = \frac{1}{nh}\sum_{i=1}^{n} K\left(\frac{D_{1,0}(x_1,x_2)}{D_{2,0}(x_1,x_2)}, \frac{D_{0,1}(x_1,x_2)}{D_{0,2}(x_1,x_2)}\frac{\boldsymbol{x}-\boldsymbol{x}_i}{h}\right)^{\top}, \tag{8}$$

~~This indicates the probable motion of the two-dimensional dynamical variable in a re-scaled temporal axis, i.e. as if the noise contributions were of identical strength, and is an effective tool to disclose the regions of convergence of the coupled system in~~ for a collection $\{\boldsymbol{x}_i\}$ of n random variables. The kernel $K(\boldsymbol{x})$ is normalisable $\int_{-\infty}^{\infty} K(\boldsymbol{x})\mathrm{d}\boldsymbol{x}=1$ and has a bandwidth h, such that $K(\boldsymbol{x})=1/h\,K(\boldsymbol{x}/h)$ (Rydin Gorjão et al., 2019; Tabar, 2019; Davis and Buffett, 2022). The bandwidth h is equivalent to the ~~two-dimensional state space.~~ selection of the number of bins, except that binning in a histogram is always "placing numbers into non-overlapping boxes". The optimal kernel is the commonly denoted Epanechnikov kernel (Epanechnikov, 1967) also used here for the analysis of the data:

$$K(\boldsymbol{x}) = \frac{3}{4}(1-\boldsymbol{x}^2), \text{ with support } |\boldsymbol{x}|<1. \tag{9}$$

Gaussian kernels are commonly used as well. Note that these require a compact support in $(-\infty,\infty)$, thus on a computer they require some sort of truncation (even in Fourier space, as the Gaussian shape remains unchanged).

~~Similarly to the one-dimensional case, one can obtain potential landscapes as integrals over the two drifts:~~

$$V_{1,0}(x_1|x_2) = -\int_{-\infty}^{x_1} D_{1,0}(x_1',x_2)\,\mathrm{d}x_1' + C(x_2),$$

$$V_{0,1}(x_2|x_1) = -\int_{-\infty}^{x_2} D_{0,1}(x_1,x_2')\,\mathrm{d}x_2' + C(x_1).$$

The selection of an appropriate bandwidth h can be aided – unlike the selection of the number of bins – by the Silverman's rule-of-thumb (Silverman, 1998), given by

$$h_\mathrm{S} = \left(\frac{4\hat{\sigma}^5}{3n}\right)^{\frac{1}{5}}, \tag{10}$$

The potential landscapes naturally emerge only in a conditional form, since $D_{1,0}(x_1,x_2)$ represents the drift of where again σ^2 is the variance of the first dynamical variable x_1 conditioned on fixed values x_2 of the second dynamical variable. Idem for $D_{0,1}(x_1,x_2)$, representing the drift of x_2 conditioned on x_1. Thus, Eqs. **??** (a) and (b) describe the deterministic motion of one variable assuming that the other variable is kept constanttime series.

The numerical analysis was

All numerical analyses were performed with `python`'s `NumPy` (Harris et al., 2020), `SciPy` (Virtanen et al., 2020), and `pandas` (Wes McKinney, 2010). Kramers–Moyal analysis was performed with `kramersmoyal` (Rydin Gorjão and Meirinhos, 2019)and `JumpDiff` **(?)**. Figures were generated with `Matplotlib` (Hunter, 2007).

The non-parametric estimates of the first KM coefficient $D_1(x)$, the associated potential landscape $V(x)$, the second KM coefficient $D_2(x)$, and the ratio of the fourth to the second KM coefficient $D_4(x)/D_2(x)$. Left column for dust, right column for δ^{18}O. Note that while the dust exhibits a bi-stable potential ((a)-(b)), the δ^{18}O exhibits a mono-stable one ((e)-(f)). The second KM coefficient $D_2(x)$ is constant in both records ((c) and (g)). The ratio $D_4(x)/D_2(x)$ is small for the dust record, yet non-negligible for the δ^{18}O, suggesting that this time series is a realisation of a discontinuous stochastic process. Details on the choice of kernel and bandwidth used for the KM coefficient estimation, as well as an analysis of the influence of the kernel bandwidth, can be found in App. A. A more detailed analysis of the second KM coefficients for both proxies can be found in App. **??**, which is supplemented by obtaining a corrective term for the Kramers–Moyal coefficients in Eq. (**??**) by extending the formal solution of the Kramers–Moyal/Fokker–Planck equation in Eqs. (**??**) and (**??**).

4 Results

This section first discusses the non-parametric estimate of the KM coefficients of the isolated dust and δ^{18}O records in a one-dimensional setting. Subsequently, the KM analysis of the two-dimensional coupled system is presented in detail.

4.1 Stability configuration and continuity of the dust and the in a one-dimensional setting

We begin by first examining the non-parametric estimates of the KM coefficients of the dust record in a one-dimensional setting. Panels (a) and (c) of Fig. 3 show the first and second KM coefficients, obtained according to will first discuss the two drift components $D_{1,0}$ and $D_{0,1}$ (see Eq. **(??)**. The reconstructed potential shown in Fig. 3 (b) exhibits two separate wells, i.e. two distinct minima. This suggests bi-stable dynamics, akin to what one observes from the trajectories of the dust record (see Fig. 1 (a) for comparison). We find the second KM coefficient to be fairly constant (Fig. 3 (c)) and the ratio between fourth and second KM coefficients to be negligible (Fig. 3 (d)), which suggests that a Langevin process with additive noise is a viable description of the isolated dust dynamics. In such a setup, the noise can stochastically induce transitions from one well to the other in qualitative agreement with the apparent sudden regime shifts observed in the record. We will revisit the continuity of the dust record after the analysis of the (5)) separately as functions of the two-dimensional space spanned by δ^{18}O in one dimension. Note that the model equations employed here are by construction symmetric with respect to time, therefore, as it is, O ratios and dust concentrations. In the model cannot reproduce the temporal asymmetry that is visually suggested in the

dust record. component-wise analysis, the analysed component takes the role of a dynamical variable, while the respective other assumes the role of a controlling parameter. In this setting, corresponding nullclines can be computed, which reveal the bifurcation and stability structure of the two individual drift components. Intersections of the two components' nullclines yield fixed points of the coupled system, which are stable if both nullclines are stable at the intersection.

We proceed with discussing analogous results for the δ^{18}O record. Fig. 3 (e) and (f) display estimates of the drift and the potential landscape for δ^{18}O, respectively. Most prominently, the drift has only a single stable fixed point (zero-crossing of the drift), or equivalently the potential function exhibits only a single well. The second KM coefficient is mostly constant, like in the case of dust (Fig. 3 (g)). With respect to the normalised units, the first and second KM coefficients of δ^{18}O exceed their counterparts for dust by factors of approximately 3-4 and 10, respectively. This indicates that δ^{18}O exhibits faster dynamics than dust. Moreover, we find that the fourth KM coefficient $D_4(x)$ for the δ^{18}O is of the same magnitude as the second KM coefficient $D_2(x)$ (

4.1 Double-fold bifurcation of the dust

The estimated dust-drift $D_{0,1}(x_1 = \delta^{18}\mathrm{O}, x_2 = \mathrm{dust})$ is displayed in Fig. 3 (h)c). This points to the potential presence of discontinuities in the record, which we will revisit shortly.

Given the high correlation between the dust and the δ^{18}O records, the differences in the reconstructed potentials and the ratio between fourth and second KM coefficient are remarkable. At first sight, the monostability of the reconstructed δ^{18}O potential contradicts the apparent two regime nature of the time series. There are two possible explanations for this discrepancy: First, regime switching of monostable stochastic process can be achieved through complex noise structures (e.g., Lévy-like noise, generalised Fokker–Planck equations, or fractal motions) (Chechkin et al., 2003, 2004; Metzler and Klafter, 2004). Secondly, a similar effect can be obtained in a two-dimensional setting if the dynamics of one dynamical variable *explicitly depends* on the other, which would be impossible to judge from the one-dimensional analysis presented so far. Thus, within the limits of this analysis – that is assuming that the process is Markovian and stationary and that the system under study is fully represented by dust and δ^{18}O (no coupling to further hidden variables) – the source of the regime switching must either be endowed by more complex noise processes or by the coupling between the dust and coefficient dictates the deterministic motion of the system along the dust direction; therein the δ^{18}O systems.

While we have found the ratio between the fourth and second KM coefficient to be negligible in the case of the dust record, for δ^{18}O our analysis yields $D_4(x)/D_2(x) \sim 1$. We remind the reader that, for a *continuous* stochastic process $x(t)$, all KM coefficients $D_m(x) = 0, m > 2$, according to Pawula's theorem. When dealing with real-world data this is never strictly the case, of course, thus examining the 'ratio of jumps to diffusive motion', that is $D_4(x)/D_2(x)$, serves only as a first indication if the process is continuous or not. Still, our results suggest that the dust record can be regarded as a realisation of a *continuous* stochastic process on the time scale of 5 yr, while the δ^{18}O is likely to comprise discontinuities on this time scale. We use the stricter Lehnertz–Tabar Q-ratio to underpin our assessment further. In Fig. **??**, we clearly see a constant relation of $Q(x,\tau)$ with respect to τ for the δ^{18}O record, suggesting that this stochastic process includes jumps. In contrast, we observe a linear relation between $Q(x,\tau)$ and τ for the dust count, suggesting a purely diffusive process without jumps. We note here that the

presence of correlated forms of noise is also sufficient to generate higher-order Kramers–Moyal coefficients (though not affect their scaling or the Q-ratio). However, we exclude this option as the auto-correlation of the increments of the data shows no correlations apart from the shortest increment, as seen in App. **??**.

The Lehnertz–Tabar Q-ratio of the dust and the δ^{18}O concentration, following Eq. (**??**), in a double-logarithmic scale. For the δ^{18}O one observes a constant relation of $Q(x,\tau)$ with τ, indicating that this time series is the realisation of a jumpy (discontinuous) processes. The dust concentration exhibits a linear relation with τ, thus is a purely diffusive process. The state x in $Q(x,\tau)$ is chosen at the maximum of the distribution of the time series.

4.2 and dust proxies in a two-dimensional setting

The different stability features in the dust and δ^{18}O observed in our one-dimensional analysis propel us to study the two proxies in a two-dimensional, coupled setting. This allows us to investigate potential couplings and, as we will show, to reconcile the two-regime nature of the δ^{18}O time series with the single potential well reconstructed in the one-dimensional analysis. In the following x_1 and x_2 refer to dust and ratio takes the role of the controlling parameter. We can trace the nullcline's branches which take a general s-shape as we vary δ^{18}O, respectively.

First we inspect the drift coefficients as before in the one dimensional setting, and reconstruct the conditional potentials according to Eq. (**??**). This yields two two-dimensional scalar fields whose physical explanatory power is limited to one direction each.

Two-dimensional PDF, potential landscapes, and vector fields. In (a) the PDF. The contour indicates a cutoff > 0.015 of the PDF, the state space we consider henceforth. The dotted elements are the records, separated into stadials (GS) and interstadials (GI). In (b) the effective vector field $\boldsymbol{F}_{\text{eff}}$ and in the inset $\boldsymbol{F}$. In (c) the potential landscape $V_{1,0}(x_1|x_2)$ of the dust, conditioned on the δ^{18}O. The inset shows $D_{1,0}(x_1,x_2)$. In (d) the potential landscape $V_{0,1}(x_2|x_1)$ of the δ^{18}O, conditioned on the dust. The inset shows $D_{0,1}(x_1,x_2)$. For $V_{0,1}(x_2|x_1)$, in (d), one finds that the location of the minimum of the landscape changes with the value of the dust conentration and undergoes no bifurcation itself. The system is always mono-stable, yet the minimum is not fixed in state space. In stark contrast, the dust landscape $V_{1,0}(x_1|x_2)$, in (c), can show up to three fixed points, depending on the value of δ^{18}O. The system exhibits a *double-fold bifurcation*, transitioning from a single (stable) fixed point for negative values of δ^{18}O, bifurcating to three fixed points (two stable), and again returning to a single (stable) fixed point for positive values of δ^{18}O This offers a good explanation of the apparent 'regime switching' in the dust record, as the system has two stable fixed points co-existing in some regions of the state space. In (b), the effective vector field shows the direction a conceptual particle follows in this two-dimensional space, telling us how δ^{18}O and dust interact and the expected trajectory the coupled system follows.

4.1.1 Double-fold bifurcation of the dust

The reconstructed conditional potential $V_{1,0}(x_1|x_2)$ of the dust is displayed in Fig. **??** (d). As a conditioned potential, it can be read by taking vertical 'slices' of the potential. Depending . Hence, depending on the value of δ^{18}O, the potential of the dust changes from a mono-stable to a bi-stable regime. Where for there are either one or three fixed points for the motion

along the dust direction: For approximately $\delta^{18}\mathrm{O} < -1.0$~~there is only~~ , there is one stable fixed point~~(a global minimum),~~ ; for approximately $-1.0 < \delta^{18}\mathrm{O} < 0.9$, there are three fixed points, two stable ones ~~(a local minimum and a global minimum)~~ and an unstable one ~~(the local maximum) between them. For~~ between them; for approximately $\delta^{18}\mathrm{O} > 0.9$, there is again just one stable fixed point~~(a global minimum~~. In fact, the merger of the nullcline's lower stable branch and unstable branch is not fully captured by the reconstruction due to too low data density (see Fig. 3 (c)). With the position of these stable fixed points depending continuously on $\delta^{18}\mathrm{O}$ ratios, we find here the characteristic form of a *double-fold bifurcation*~~. Fig. ?? (d) suggests that the second bifurcation ($\delta^{18}\mathrm{O} = 0.9$) is in fact located at a slightly higher value, since the merger of the upper stable branch and the unstable branch is not fully covered by the reconstruction~~, in which $\delta^{18}\mathrm{O}$ takes the role of a control parameter.

~~In such a setting, abrupt transitions as those observed in the dust record can happen~~ The dust nullclines' structure supports the possibility for abrupt transitions in two ways: ~~either~~ Either random fluctuations move the system across the unstable branch (if present, depending on the value of the control parameter) or the control parameter, in this case ~~the~~ $\delta^{18}\mathrm{O}$, crosses a bifurcation point and the currently attracting stable ~~fixed point is dissolved~~branch merges with the unstable branch. In both cases, the system will transition fairly abruptly to the alternative stable branch. Rate-induced tipping seems ~~unlikely~~ implausible in this case, since the unstable branch is ~~mostly a~~ approximately constant with respect to a change of the control parameter (i.e. $\delta^{18}\mathrm{O}$). ~~This structure prevents to cross~~ Thus, a crossing of the unstable branch by means of a rapid shift in $\delta^{18}\mathrm{O}$ is almost impossible.

4.1.1 ~~Coupling of the drift with the dust~~

~~We now turn our attention to~~

4.2 Coupling of the $\delta^{18}\mathrm{O}$ drift with the dust

We now focus on the reconstructed drift $D_{1,0}(\delta^{18}\mathrm{O}, \mathrm{dust})$ of the $\delta^{18}\mathrm{O}$ ~~variable. In~~ ratios (Fig. ??3 (~~c)we present the reconstructed potential $V_{0,1}(x_2|x_1)$ for~~ d)). Its nullcline appears to be an explicit function of the dust, i.e. for each value of dust concentrations there is a single stable fixed point along the δ^{18}~~O, conditioned on the value x_1 for the dust . Taking a horizontal 'slice' we recover a parabolic shape with a single minimum. Qualitatively, this feature is preserved across the entire range of potential conditioning dust values. However, the~~ O-dimension. The position of the ~~minimum $\delta^{18}\mathrm{O}^*$ appears to be determined by the~~ fixed point changes with the value for dust in a continuous manner, with a high rate of change for intermediate dust values ~~whilst no~~ and small change for more extreme dust values. ~~Our finding of δ^{18}O following~~ These findings suggest that $\delta^{18}\mathrm{O}$ follows a mono-stable process ~~is thus confirmed in the two-dimensional analysis, with the added feature that the potential minimum's position~~ whose fixed point is subject to change in response to an 'external control' imposed by the dust.

~~In summary, in~~

4.3 Combined two-dimensional drift

Fig. 3 (b) shows the two-dimensional ~~analysis the monostability of the δ^{18}O and the bistability of the dust found in the one-dimensional analysis remain preserved.We find a continuous dependency of the position of the stable δ^{18}O fixed point~~

~~on the dust. In contrast, a breakdown~~ drift field $\boldsymbol{F}(\delta^{18}\mathrm{O}, \mathrm{dust})$ of the coupled system given by Eq. (5). The two fixed points which arise from the intersections of the dust ~~'s bistability for extreme values of δ^{18}O can be observed. These findings are consistent with the observed regime switching of both records, which we struggled to reconcile with the results obtained from the one-dimensional analysis. If attracted by the upper stable branch, the dust assumes values on the order of ~ 0.5. This implies a~~ nullcline's stable branches with the δ^{18}O stable ~~fixed point position of ~ -0.6. A transition in the dust to the lower stable branch associated with dust values ~ -0.5 shifts the stable fixed point of δ^{18}O to ~ 0.6. The bistability embedded in the potential governing the dust is thus transferred to the δ^{18}O and provides an explanation for the observed regime switches of the record~~nullcline fall well within the regions of the state space associated with Greenland stadials and interstadials, respectively. The stable regime (δ^{18}O ~~~ -1.5, dust ~ 1~~ ~ -1, dust ~ -1) can be identified with Greenland stadials, while the stable regime (δ^{18}O ~~~ 2, dust ~ -1~~ ~ 0.5, dust ~ 1) corresponds to Greenland interstadials.

~~The study of the conditional potentials provided insight in the underlying static stability configuration of the coupled δ^{18}O–dust system. However, to gain a more specific understanding of the dynamics, we investigate the (effective) vector field of motion $\boldsymbol{F}$ ($\boldsymbol{F}_{\mathrm{eff}}$) in the next step.~~

~~For each point in state space, the vector field $\mathbf{F}(x_1, x_2) = (D_{1,0}(x_1, x_2), D_{0,1}(x_1, x_2))^\top$ indicates the expected direction of movement of the system (see inset of~~ Similarly, we can locate an unstable fixed point roughly in between the two observed stabled fixed points of the coupled system. Judging from Fig. **??**3 (b) ~~). One can see that the restoring force in~~ the unstable fixed point resembles a saddle with convergent drift along the δ^{18}O direction ~~substantially exceeds the one in the dust direction. This is in line with the magnitude of both the first and second KM coefficients obtained in the one-dimensional analysis (see~~ and divergence along the connection line between the two stable fixed points. The system's bistability is inherited from the dust's drift and is not enshrined in the δ^{18}O ratios. As mentioned previously, Fig. 3~~) and points to a time scale separation in the dynamics of the coupled system . In~~ (b) suggests that – starting from a stable fixed point – perturbations along the δ^{18}O direction will not entail state transitions but instead simply decay until the system reaches the δ^{18}O ~~direction strong fluctuations are quickly compensated by a strong restoring force. In~~ nullcline again. In contrast, perturbations along the dust direction ~~, however, the fluctuations and the restoring force are smaller than that of the δ^{18}O, while the ratio between noise and drift is comparable in both directions. This can be interpreted as a time scale separation with fast dynamics happening along the δ^{18}O dimension.~~ may shift the system into the respective other basin of attraction.

4.4 Rotation of the state space and the presence of a non-negligible interplay of the dust and δ^{18}O

Above we argued for the existence of a double-fold bifurcation in the dust variable. In order to ~~make the dynamics along the dust direction visible, we rescale the two-dimensional potentials in relation to their diffusion (the second Kramers–Moyal coefficients $D_{2,0}$ and $D_{2,0}$). The effective vector field $\mathbf{F}_{\mathrm{eff}}$, obtained according to Eq. (**??**), is displayed in~~ show that the coupling of the dust and δ^{18}O is not a spurious result of the initial state space, we conduct an analogue analysis using a rotated state space. To rotate the state space we employ principal component analysis and obtain a new set of variables $\boldsymbol{p} = (p_1, p_2)$,

with $\boldsymbol{p} = \mathbf{U}(\delta^{18}\mathrm{O}, \mathrm{dust})^\top$, where $\mathbf{U}$ is given by

$$\mathbf{U} = \begin{bmatrix} -0.707 & -0.707 \\ -0.707 & 0.707 \end{bmatrix}. \tag{11}$$

In Fig. ?? (b).While in the un-scaled vector field $\mathbf{F}$ the influence of the dust drift on the coupled system is practically hidden by strength of 4 we redraw Fig. 3 in the rotated state space; we observe that (i) the nullcline of p_1 is now almost independent of p_2 and (ii) the p_2-nullcline is still strongly dependent on p_1, while none of the rotated variables shows any bifurcation. Overall, the dynamics of the dust–δ^{18}O drift, we can now observe more complex structures in the effective vector field. Two main regions of convergence can easily be identified around ($\delta^{18}\mathrm{O} \sim -0.6, \mathrm{dust} \sim 0.5$) and ($\delta^{18}\mathrm{O} \sim 0.6, \mathrm{dust} \sim -0.5$) which correspond to Greenland stadials and interstadials, respectively, as mentioned previously. These convergent regions consistently coincide with the two maxima in the O can be explained as we introduced in Sec. 4.2 with two basins of attraction being separated by a saddle. In particular, the assessment of the drift in the rotated state space shows, that the data cannot be described by a simple two-dimensional density shown in Fig. ?? (a). The effective vector field of motion does not indicate a clear path that the system would take in order to transition between stadial and interstadial states. This leaves open the possibility that transitions between stadial and interstadial states are mainly induced by noise as argued by, e.g., Ref. (Ditlevsen et al., 2007) (i.e. noise-induced tipping), facilitated by a shallow potential barrier close to the minima of the (effective) vector field. double-well potential with two axes of symmetry and decoupled dynamics along these.

5 Discussion

We have used the one and two-dimensional Kramers–Moyal equation to investigate the deterministic drift of the combined dust and δ^{18}O record from the NGRIP ice core for the time interval 59–27 kyr b2k, which exhibits pronounced DO variability. The approach was chosen to disclose the dynamical features of this two-dimensional system. In the following, we discuss how our study relates to previously published investigations of the same data and how it contributes to the broad discourse on DO variability.

Although we obtain slightly different and in parts opposing result, our study ties in naturally with previous data-driven analysis of Greenland ice core proxy data. After the work presented by Boers et al.(Boers et al., 2017) it is only the second study to follow a two-dimensional inverse modelling approach with respect to Greenland ice core data.

Adopting a Langevin-type approach (Ditlevsen, 1999) found the calcium record from the GRIP ice core (Fuhrer et al., 1993) with annual resolution to be consistent with a bi-stable drift term and α-stable noise. We cannot confirm the presence of α-stable noise in the dustrecord – which is often regarded as an equivalent to calcium – from the NGRIP ice core. This might be due to reconstructed stability structure with two basins of attraction and a separating saddle is consistent with the regime switches observed simultaneously in both components of the record: in the δ^{18}O-dust plane the basins of attraction are located such that a transition from one to the other entails a change in both components. However, the analysis of the lower resolution of vector field (Fig. 3 (b)) does not indicate any clear paths the system takes in order to transition between stadial and interstadial

states. The shape of the nullclines can, in principle, allow for a situation where a perturbation along the δ^{18}O direction pushes the dust across its bifurcation point, triggering a transition of the ~~data analysed here~~dust, which in turn stabilises the δ^{18}O perturbation. The combined drift $\boldsymbol{F}(x_1, x_2)$, however, exhibits strong restoring forces along the δ^{18}O direction which render this mechanism rather implausible. Viewed from either stable fixed point, perturbations along the dust direction could in contrast push the system across the basin boundary relatively easily. Certainly, a combination of noise along both directions may also be able to drive the system across the region of weak divergence that separates the two attractors. We note that the mild relaxation that is typical for Greenland interstadials cannot be explained from results of this analysis alone.

~~Livina *et al.* (Livina et al., 2010) reported on a changing number of stable states detected in one-dimensional GRIP and NGRIP δ^{18}O and~~GRIP calcium data ~~with 20 yr and annual resolution, respectively. Their analysis attests bistability of~~ In the following we discuss how the results shown here relate to the findings of previous studies. An important branch of research around DO events draws on low-dimensional conceptional modelling and, related to that, inverse modelling approaches with model equations being fitted to ice core data. Many of these studies build on stochastic differential equations and in particular on Langevin-type equations. Our study follows the same key paradigm, regarding the paleoclimate record as the realisation of a stochastic process. However, as far as we know, it is the first study to assess the two-dimensional drift non-parametrically in the δ^{18}~~O record for~~ O-dust plane.

For the period investigated here ~~for bothice cores. However, throughout the last glacial maximum~~ Livina et al. (2010) individually attested bistability to both, the δ^{18}O and the dust component by fitting a Langevin process to a 20-year mean version of the NGRIP record. Later Kwasniok (2013) and Lohmann and Ditlevsen (2018a) showed – ~~which we intentionally excluded from our study~~ using techniques from Bayesian model inference – ~~Livina *et al.* (Livina et al., 2010) find monostability consistently in all three time series. Assuming a stationary process for the period 60–20 kyr b2k, the bistability of~~ that a two-dimensional relaxation oscillator model outperforms a simple double-well potential in terms of simulating the NGRIP δ^{18}O record. Such a relaxation oscillation still relies on a fundamental bistability in the variable that is identified with δ^{18}O ~~potential was later confirmed by Kwasniok (Kwasniok, 2013) based on 50 yr resolution data from NGRIP and GRIP.~~ ratios. A physical interpretation for an FitzHugh—Nagumo-type DO model is provided by Vettoretti et al. (2022).

~~Our results suggest that the two regime nature is probably not an intrinsic feature~~ Our results contradict the interpretation that δ^{18}O ratios and therewith Greenland temperatures bear an intrinsic bistability. In the two-dimensional setting, the apparent two-regime nature of the δ^{18}O ~~, but rather an effect of the coupling to other climate variables. Assuming that~~ record can be explained by the control that the dust exerts on the δ^{18}O ~~exclusively represents local temperatures, this result seems reasonable as one would not expect two distinct stable temperature regimes with all controlling factors kept fixed . In contrast, considering the position of the jet stream a dynamical bistability is far more plausible and could explain the~~ fixed points and the corresponding location of the two stable fixed points in the two-dimensional drift.

Since we find the bistability of the ~~dust record found in this study. We note that the bistability of jet stream has been evidenced~~ reconstructed coupled system rooted in the dust, our analysis suggests that the atmosphere may have played a more active role in stabilising the two regimes that dominated the last glacial's Northern Hemisphere climate than many AMOC-based explanations of the DO variability suggest (Ganopolski and Rahmstorf, 2002; Clark et al., 2002; Vettoretti and Peltier, 2018; Li and Born,

. Similarly, the observation that dust-perturbations may induce state transitions may be seen as a hint that random perturbation of the atmospheric circulation can trigger DO events as proposed e.g. by Kleppin et al. (2015). In this regard, it should be noted that a multistability of the latitudinal jet stream position has been suggested – although in a somewhat different setting and sense – ~~in~~ based on an investigation of reanalysis data of modern climate (Woollings et al., 2010). ~~Evidently, our analysis is limited to solely two climate proxy variables and the stability of the one can only be assessed conditioned on the other, leaving aside potential coupling to further external factors. Yet our results question the prevailing perception of the~~ In contrast, one would not expect two distinct stable Greenland temperature regimes with all controlling factors kept fixed. This is in line with the bistability of the dust-drift and the monostable δ^{18}O ~~record as~~ -drift revealed in our analysis.

Clearly, the state space spanned by δ^{18}O and dust is a very particular one. On the one hand the interpretation of the two proxies as indicators of Greenland temperatures and the hemispheric circulation state of the atmosphere bears qualitative uncertainties and should certainly not be considered a one-to-one mapping. On the other hand, other climate subsystems not directly represented in the ~~signature of an intrinsically bistable process. This is at least partly in line with the findings of Lohmann et al. (?), who have shown that a fast-slow limit cycle model outperforms a simple double wellmodel~~ data analysed here, like the AMOC for example, are likely to have played an important role in the physics of DO variability as well. Even if δ^{18}O ~~is identified with the model's fast component.~~

~~Boers *et al.* (Boers et al., 2017) were the first to study~~ ratios and dust concentrations were to exclusively represent Greenland temperatures and the atmospheric circulation state, the recorded climate variables were certainly highly entangled with other climate variables such as the AMOC strength, the Nordic Sea's and North Atlantic's sea ice cover, or potentially North American ice sheet height (e.g. Menviel et al., 2020; Li and Born, 2019; Boers et al., 2018; Zhang et al., 2014; Dokken et al., 2013) . In our analysis, such couplings are subsumed in the δ-correlated noise term $\boldsymbol{\xi}$ – an approach which may rightfully be criticised to be overly simplistic. However, given the lack of climate proxy records that jointly represent more DO-relevant components of the climate system on the same chronology, the chosen method reasonably complements existing data-driven investigations of DO variability. For example Boers et al. (2017) similarly examined the dynamical features of the combined δ^{18}O–dust record. They proposed a third-order polynomial two-dimensional drift in combination with a non-Markovian term and Gaussian white noise to model the coupled dynamics. While our approach is limited to a Markovian setting, it allows for more general forms of ~~the drift and of the noise. In particular, we have shown that the δ^{18}O record cannot be treated as a time-continuous process. The non-vanishing fourth KM coefficient in the δ^{18}O, which indicates forcing beyond typical Gaussian white noise, could point to an external trigger that directly acts on the Greenland temperatures. A sudden shift in the latter could then entail a regime switch in the atmospheric configuration. However, the interpretation of the fourth KM coefficient is not straightforward and depends on the exact choice of the stochastic process model . The role of discontinuities in the δ^{18}O record merits further investigation. Moreover, it should be mentioned that non-Markovian processes, as proposed in Ref. (Boers et al., 2017), can also give rise to higher-order KM coefficients.~~

~~The results obtained in our analysis do not give a clear answer to the question for the exact mechanism that triggered DO events.In principle, the revealed double-fold bifurcation would allow for bifurcation-induced transitions and thus for a limit-cycle behaviour.However, the record show that system does not track the stable fixed point branches until the bifurcation~~

points, but tends to transition earlier (not shown) . Also, the structure of the δ^{18}O drift is incompatible with a deterministic cyclic motion in the dust-δ^{18}O plane. In fact, the specific structure of the double-fold bifurcation leaves room for a weak barrier between stadial and interstadial states in the vicinity of the bifurcation point, thus creating a 'channel'-like passage, through which the system passes.

We conclude therefore that – based on our results – the DO transitions are to large degree induced by noise, acting on the background of a double-fold dynamicsgoverning the dust, for which the δ^{18}O acts as control parameter. These finding do not contradict previous studies that proposed limit-cycle models to explain the δ^{18}O record, since the cyclic motion was not expected to happen in a state space comprised of Greenland temperatures and atmospheric large scale circulation (Kwasniok, 2013; **?**)drift (and noise). Being non-parametric, it does not rely on prior model assumptions in this regard. It is not per se clear how the couplings to 'hidden' climate variables (i.e., those not represented by the analysed proxy record) influence the presented drift reconstruction and there is certainly a risk of missing a relevant part of the dynamics.

6 Conclusion

In this article, we We have analysed the records of δ^{18}O ratios and dust concentrations from the NGRIP ice core from a data-driven perspective (Ruth et al., 2003; North Greenland Ice Core Projects members, 2004; Gkinis et al., 2014). The central point of our study was to examine the stability configuration of the coupled δ^{18}O–dust process by reconstructing its potential landscape. For this aim we utilised the Kramers–Moyal equation which generalises the Fokker–Planck equation in the sense that higher-order Kramers–Moyal coefficients can be related to discontinuities in the stochastic processes.

In a first step, a standard one-dimensional Kramers–Moyal analysis revealed a monostable potential for the isolated δ^{18}O record and a bistable one for the dust. This finding calls the prevailing understanding that the Greenland ice core δ^{18}O record stem from bistable dynamics into question. The qualitative difference between the reconstructed potentails is remarkable given the high co-variability of the two time series and their synchronous two-regime character, which dominates not only the dust but also the δ^{18}O record. Moreover, we found non-vanishing higher-order Kramers–Moyal coefficients for δ^{18}O, indicating the presence of discontinuities in the record, assuming the process is truly Markovian. This renders the Langevin equation unsuited to fully describe the underlying process and requires the addition of jumps. In contrast, according to our analysis, the isolated dust record is a continuous process that is described well by the Langevin equation.

In a second step, we expanded our analysis to a two-dimensional setting that takes into account possible couplings between the δ^{18}O and dust time series. Our two-dimensional examination of the conditioned potential landscapes confirms our initial finding of drift. Our findings indicate a mono-stable potential for the δ^{18}O, wherein the minimumO-drift whose fixed point's position is controlled by the value an explicit function of the dust. The dust variable, on the other handin contrast, seems to undergo a *double-fold bifurcation* parametrised by the parameterised by δ^{18}O, where we can observe the with a change from a single (stable) fixed point to three fixed points (two stable, one unstable), and again to a single (stable) fixed point, from small to large values of the δ^{18}O . Our analysis reveals two ratio. Together, the drift components yield two stable fixed points in the coupled system surrounded by convergent regions in the δ^{18}O–dust state space, in agreement with the two-regime nature of the

coupled record. Judging from the reconstructed drift, perturbations along the dust dimension are more likely to trigger a state transition, which points to an active role of the atmospheric circulation in DO variability.

Importantly, our findings question the prevailing interpretation of the two regimes observed in the isolated δ^{18}O record as the direct signature of an ~~intrinsically bistable process~~intrinsic bistability. Such an intrinsic bistability can be confirmed only for the dust variable. Regarding δ^{18}O ratios as a direct measure of the local temperature, it seems plausible that not the temperature itself is bistable, but rather that the bistability is enshrined in another climate variable – or an at least regional-scale climate process or a combination of processes – that drives Greenland temperatures. The apparent two-regime nature of the δ^{18}O record would thus only be inherited from the actual bistability of other processes. This may be the atmospheric circulation as represented by the dust proxy, or another external driver ~~whose signature might be encoded in the higher-order KM coefficients of the δ^{18}O.~~

~~Many physical mechanisms have been proposed as candidates for explaining the DO events, with most of them building on the proposed bistability of the Atlantic Meridional Overturning Circulation (AMOC), e.g., Refs. (Ganopolski and Rahmstorf, 2001; Clark e . While some studies argue that DO cycles are the signature of self-sustained oscillations within the coupled sea-ice ocean system (Boers et al., 2018; Vettoretti and Peltier, 2018; Menviel et al., 2020), others advocate for an active role of the atmosphere or even ice sheets in the initialisation of DO events, e.g., Refs. (Kleppin et al., 2015; Zhang et al., 2014; Gottwald, 2020). The proposed self-sustained oscillation mechanism is not contradicted by our investigation and neither is a stochastic trigger embedded in the sea ice. Our results do also not contradict an atmospheric trigger for the DO events – we see that if the dust switches from one state to the other this will in turn shift the level of the δ^{18}O. Yet, the atmospheric transitions would in this picture not be induced by rare extreme events as proposed by Ditlevsen (Ditlevsen, 1999), but rather by a regular additive Gaussian noise. However, as mentioned previously, the absence of discontinuities in the dust record may also be a question of the temporal dataresolution~~not directly represented by the analysed data.

~~Certainly, DO events and their global expression feature a complex interplay of the AMOC, the North Atlantic and Nordic Sea's sea ice cover, the polar jet stream and probably more climatic subsystems such as ice sheets or the East Asian Monsoon system (Cheng et al., 2013). Our analysis considered only a two-dimensional projection of the very high-dimensional dynamics and can therefore not be expected to deliver all details of the triggering mechanism. Neither the ocean-focused self-sustained oscillation hypothesis, nor the idea that the atmosphere acts as a trigger, can be ruled out based on our findings. Nevertheless, our results challenge prevailing assumptions, e.g., regarding the bistability and the smoothness of the temperature proxy record and adds valuable information that may help further constrain physical hypotheses to explain the DO events in the future. Analysis structurally similar to this one~~

Similar investigations to ours should be applied to other pairs of Greenland proxies to investigate the corresponding two-dimensional drift. Finally, our study underlines the need for ~~higher resolution~~ higher-resolution data, as the scarcity of data points is a limiting factor for the quality of non-parametric ~~estimate~~ estimates of the KM coefficients.

Code availability. The code used for this study will be made available by the authors upon request.

7 Data detrending

As mentioned in Sec. 2, this study focuses on the period 59–27 kyr b2k. Detrending of the data is needed to ensure that the time series can be considered stationary processes, which is an underlying assumption for the Kramer–Moyal analysis performed in our investigation. To compensate for the influence of the background climate on the climate proxy records of dust and δ^{18}O, we remove a linear drift with respect to reconstructed global average surface temperatures (Snyder, 2016) from both time series. Fig. **??** illustrates the detrending scheme for both time series. Due to the two regime nature of the time series, a simple linear regression overestimates the temperature dependencies (see Fig. **??**(c) and (d), dashed line). Instead, we separate the data from Greenland Stadials and Greenland Interstadials and then minimise the expression

$$\left(\sum_{i=1}^{N} \left(\delta^{18}\mathrm{O}(t_i) - a\Delta T(t_i) - \begin{cases} b_{\mathrm{GI}}, \text{ if } t_i \in \mathrm{GI} \\ b_{\mathrm{GS}}, \text{ if } t_i \in \mathrm{GS} \end{cases} \right)^2 \right)^{1/2},$$

with respect to the parameters a, b_{GI}, and b_{GS} (correspondingly for dust). $t_i \in$ GS (GI) indicates that a given time t_i falls into a Stadial (Interstadial) period. The index i runs over all data points and N denotes the total number of points. The resulting a is used to detrend the original data with respect to the temperature. The detrended data is then normalised by subtraction of its mean and division by the difference between the mean Stadial and mean Interstadial values.

Removal of a linear trend in the NGRIP δ^{18}O and dust time series (North Greenland Ice Core Projects members, 2004) with respect to a global average surface temperature reconstruction (Snyder, 2016). In panel (a) both original δ^{18}O (blue) as well as detrended and normalised (purple) are shown. Idem for the dust record in panel (b) (dark green and light green, respectively). The background temperature given in anomalies to present day climate is shown in both aforementioned panels (red). Panels (c) and (d) show a scatter plot the original δ^{18}O and dust data with respect to temporarily corresponding temperature anomalies, respectively. Data from Interstadials (Stadials) is shown in orange (light blue). The black dashed line results from a simple linear fit to the entire data, while the continuous black lines correspond to the fitting scheme that uses a single slope but two different offsets to separately fit the Stadial and Interstadial data.

7 Markov property of the data

The Markov property of the data, central in this work, is a necessary property whilst designing Markovian stochastic models to describe any paleo-climatic data, as the name suggests. These include the most commonly used stochastic models, e.g., Langevin processes, based on having independent increments of the data (Risken and Frank, 1996; Friedrich et al., 2011). This is best understood by examining the Chapman–Kolmogorov equation of the joint probability densities $p_{i_1,\ldots,i_n}(x_1,\ldots,x_n)$, with $\{x_i\}$ a collection of random variables ordered with $t_1 < \cdots < t_n$

$$p_{t_1,\ldots,t_n}(x_1,\ldots,x_n) = p_{t_1}(x_1)p_{t_2;t_1}(x_2 \mid x_1)\cdots p_{t_n;t_{n-1}}(x_n \mid x_{n-1}),$$

where the Markov property here allows us to separate each joint probability density as being solely a function of two adjacent segments. One of the most straightforward ways of evaluating the Markov property for data is to examine the auto-correlation function of the increments of the data at the shortest incremental distance. That is, take the data x_t, construct the differences $\Delta x_t = x_{t+1} - x_t$, and obtain the auto-correlation function $\rho(\tau)$

$$\rho(\tau) = \frac{\mathrm{E}\left[(\Delta x_t - \mu_t)(\Delta x_{t+\tau} - \mu_{t+\tau})\right]}{\sigma_t \sigma_{t+\tau}},$$

here μ is the mean and σ^2 the variance of Δx_t. In Fig. **??** we display the auto-correlation functions $\rho(\tau)$ of the two time series, which is only lightly anti-correlated at the shortest lag of $\tau = 5y$.

Here, we include a small note of caution for the interested reader. Pre-processing paleo-climatic data is usually implemented to reduce the noise or remove short or long term trends. A common method to remove long-term trends in the records is to apply a low-pass filter. This will invariantly lead to spurious correlations, thus it should be considered with care, dependent on the data analysis techniques employed. In our case, this would be disastrous. Low-pass filtering the data would create spurious correlations in the incremental time series and Markovianity would be lost.

Autocorrelation $\rho(\tau)$ of the increments Δx_t of δ^{18}O and dust records. Both records show a weak anti-correlation at the shortest lag $\tau = 5y$, and no correlation for $\tau > 5y$. We thus consider the data Markovian.

Data availability. All ice core data was obtained from the website of the Niels Bohr Institute of the University of Copenhagen (https://www.iceandclimate.nbi.ku.dk/data/); the detailed links are indicated below. The original measurements of δ^{18}O ratios and dust concentrations go back to (North Greenland Ice Core Projects members, 2004) and (Ruth et al., 2003), respectively. The 5 cm resolution δ^{18}O ratio and dust concentration data together with corresponding GICC05 ages used for this study can be downloaded from https://www.iceandclimate.nbi.ku.dk/data/NGRIP_d18O_and_dust_5cm.xls (last access: 11. August 2022). The δ^{18}O data shown in Fig. 1 with 20 yr resolution that cover the period 122–10 kyr b2k are available from https://www.iceandclimate.nbi.ku.dk/data/GICC05modelext_GRIP_and_GISP2_and_resampled_data_series_Seierstad_et_al._2014_version_10Dec2014-2.xlsx (last access: 08.08.2022) and were published in conjunction with the work by Rasmussen et al. (2014) and Seierstad et al. (2014). The corresponding dust data, also shown in Fig. 1 and covering the period 108–10 kyr b2k, can be retrieved from https://www.iceandclimate.nbi.ku.dk/data/NGRIP_dust_on_GICC05_20y_december2014.txt. The global average surface temperature reconstructions provided by Snyder (2016) and used here for the detrending were retrieved from https://static-content.springer.com/esm/art%3A10.1038%2Fnature19798/MediaObjects/41586_2016_BFnature19798_MOESM258_ESM.xlsx (last access: 08.08.2022)

7 Nadaraya–Watson estimator of the Kramers–Moyal coefficients and bandwidth selection

In order to carry out the estimation in Eq. **??** we map each data point in the corresponding state space to a kernel density and then take a weighted average over all data points

$$D_m(x) \sim \frac{1}{m!}\frac{1}{\Delta t}\langle (x(t+\Delta t)-x(t))^m | x(t)=x\rangle$$
$$\sim \frac{1}{m!}\frac{1}{\Delta t}\frac{1}{N}\sum_{i=1}^{N-1} K(x-x_i)(x_{i+1}-x_i)^m.$$

Alike selecting the number of bins in a histogram, when employing kernel-density estimation with an Nadaraya–Watson estimator for the Kramers–Moyal coefficients $D_m(x)$, one needs to select both a kernel and a bandwidth (Nadaraya, 1964; Watson, 1964; La
. Firstly, the choice of the kernel is the choice of a function $K(x)$ for the estimator $\widehat{f}_h(x)$, where h is the bandwidth at a point x

$$\widehat{f}_h(x) = \frac{1}{nh}\sum_{i=1}^{n} K\left(\frac{x-x_i}{h}\right).$$

for a collection $\{x_i\}$ of n random variables. The kernel $K(x)$ is such that $K(x) = 1/hK(x/h)$ and is normalisable $\int_{-\infty}^{\infty} K(x)\mathrm{d}x = 1$ (Tabar
. The bandwidth is equivalent to the selection of the number of bins, except that binning in a histogram is always "placing numbers into non-overlapping boxes". The optimal kernel is the commonly denoted Epanechnikov kernel (Epanechnikov, 1967) , but Gaussian kernels can be used as well. These nevertheless require a compact support in $(-\infty,\infty)$, thus on a computer they require some sort of truncation (even if Fourier space, as the Gaussian shape remains unchanged).

The selection of an appropriate bandwidth h can be aided – unlike the selection of the number of bins – by the Silverman's rule-of-thumb (Silverman, 1998), given by

$$h_{\mathrm{S}} = \left(\frac{4\hat{\sigma}^5}{3n}\right)^{\frac{1}{5}},$$

where again σ^2 is the variance of the time series. In Fig. **??** three different bandwidths are used to evaluated the various KM coefficient, as given in Fig. **??** The bandwidths are the optimal bandwidth given by the Silverman's rule-of-thumb h_{S}, three times h_{S}, and one-third h_{S}.

The effect of the bandwidth selection h_{S} on the KM estimations, in identical fashion to Fig. 3. The non-parametric estimates of the first KM coefficient $D_1(x)$, the associated potential landscape $V(x)$, the second KM coefficient $D_2(x)$, and the ratio of the fourth to the second KM coefficient $D_4(x)/D_2(x)$. Left column for dust, right column for δ^{18}O. Three bandwidths used for the Nadaraya–Watson kernel-density estimator: the optimal Silverman's rule-of-thumb h_{S}, three times h_{S}, and one-third h_{S}. The Nadaraya–Watson kernel-density estimator's bandwidths h_{S} for δ^{18}O is 0.131 and for dust 0.103. In all cases, the interpretation of the estimator remains the same: bi-stability in the dust, mono-stability in the δ^{18}O. In (c) and (g) are included the first-order estimator for the second KM coefficient $D_2(x)$, i.e. without corrective terms, discussed in App. **??**.

Note that in neither of the examples with different bandwidths we notice a change of the potential shape of the various records. The mono-stability of the potential $V(x)$ of δ^{18}O is persistent, as is the bi-stability of the potential $V(x)$ of the dust concentration.

7 Second-order correction to the Fokker–Planck/Kramers–Moyal operator

In order to correctly retrieve from data the Kramers–Moyal coefficients, we need to evaluate the operation in the Fokker–Planck equation Eq. (??). In fact, we showed that this equation is not sufficient to describe the fast transitions in the δ^{18}O record. Let us nevertheless focus on this equation for the moment, and rewrite it in a more formal manner as an operator

$$\begin{aligned}\frac{\partial}{\partial t}p(x,t+\tau|x',t) &= \tfrac{\partial}{\partial x}D_1(x)p(x,t+\tau|x',t)\\ &\quad +\tfrac{\partial^2}{\partial x^2}D_2(x)p(x,t+\tau|x',t)\\ &= \mathcal{L}_{\mathrm{FP}}\, p(x,t+\tau|x',t),\end{aligned}$$

with $\mathcal{L}_{\mathrm{FP}}$ the formal Fokker–Planck operator and

$$D_m(x) = \frac{1}{m!}\lim_{\tau\to\infty}\frac{M_m(x,\tau)}{\tau},$$

where $M_m(x,\tau)$ is the m-order conditional moment, i.e.

$$M_m(x,\tau) = \int_{-\infty}^{\infty}(x'-x)^m p(x',t+\tau|x,t)\,\mathrm{d}x'.$$

which we introduced in Eq. (??) in a similar notation. If we limit $m \leq 2$, we are truly talking about a Langevin process described by the Fokker–Planck equation, with $\mathcal{L}_{\mathrm{FP}}$ the formal Fokker–Planck operator. We also saw that we can generalise the problem and not truncate the terms at second order, thus including an infinite series of conditional moment $M_m(x,\tau)$ would give rise to the Kramers–Moyal equation and the Kramers–Moyal operator $\mathcal{L}_{\mathrm{KM}}$. The subsequent second-order correction is showcased here for the Fokker–Planck equation, based on Ref. (Gottschall and Peinke, 2008; Rydin Gorjão et al., 2021). For sake of coherence, we utilise here the second-order corrections to show that the second Kramers–Moyal coefficient – the diffusion strength – can be seen as constant, i.e. not state depended.

In order to solve Eq. (??), one takes the formal step considering an initial conditions $\delta(x-x')$ as a starting point and employing the exponential representation of the operator, which we can decompose it into a power series as

$$\begin{aligned}p(x,t+\tau|x',t) &= \exp\left(\tau\mathcal{L}_{\mathrm{FP}}\right)\delta(x-x')\\ &= \textstyle\sum_{k=0}^{\infty}\frac{(\tau\mathcal{L}_{\mathrm{KM}})^k}{k!}\delta(x-x').\end{aligned}$$

From here we consider the first-order and second-order approximation, i.e. truncation of the operator, as

$$\exp\left(\tau\mathcal{L}_{\mathrm{FP}}\right) \sim 1+\tau\mathcal{L}_{\mathrm{FP}}+\frac{\tau^2}{2}\mathcal{L}_{\mathrm{FP}}\mathcal{L}_{\mathrm{FP}}+\mathcal{O}(\tau^3).$$

Considering only the first-order, $\sim\tau$, we recover the well-known relation between the conditional moments and the Kramers–Moyal coefficients, given by

$$D_m(x) = \lim_{\tau\to 0}\frac{M_m(x,\tau)}{(m!)\tau}.$$

If we now include the second-order approximation, i.e. we consider terms up to $\sim \tau^2$, we obtain a corrective term for the second Kramers–Moyal coefficient

$$D_1(x) = \lim_{\tau \to 0} \frac{1}{\tau} M_1(x, \tau),$$
$$D_2(x) = \lim_{\tau \to 0} \frac{1}{2\tau} \left(M_2(x, \tau) - M_1(x, \tau)^2 \right).$$

We employ this correction to our examination to show that the diffusion coefficient, i.e. the amplitude of the fluctuations, is constant in space. In Fig. **??**(c) and (g) we display both the first-order and the corrected, second-order diffusion coefficient. In this we can see that utilising solely the first-order correction could lead us to erroneously consider the diffusion term as state dependent (having a parabolic shape), suggesting a multiplicative noise. By implementing the second-order corrective terms a considerable improvement of the estimation is achieved, to what we judge to be simple additive (not state dependent) noise in the records.

Appendix A: Nadaraya–Watson estimator of the Kramers–Moyal coefficients and bandwidth selection

Author contributions. KR and LRG designed the study with contributions from all authors. KR and LRG conducted the numerical analysis. KR and LRG wrote the paper with contributions from all authors.

Competing interests. No competing interests

Acknowledgements. LRG and DW gratefully acknowledge support from the Helmholtz Association via the grant *Uncertainty Quantification – From Data to Reliable Knowledge (UQ)* with grant agreement no. ZT-I-0029. This work was performed by LRG as part of the Helmholtz School for Data Science in Life, Earth and Energy (HDS-LEE). NB acknowledges funding by the Volkswagen foundation. This is TiPES contribution #XX; the Tipping Points in the Earth System (TiPES) XXX; the *Tipping Points in the Earth System (TiPES)* project has received funding from the European Union's Horizon 2020 research and innovation programme under grant agreement no. 820970. Further funding was received from the European Union's Horizon 2020 research and innovation programme under the Marie Skłodowska-Curie grant agreement No. 956170 Funded by the Deutsche Forschungsgemeinschaft (DFG, German Research Foundation), grant no. 491111487.

References

Andersen, K. K., Svensson, A., Johnsen, S. J., Rasmussen, S. O., Bigler, M., Röthlisberger, R., Ruth, U., Siggaard-Andersen, M. L., Peder Steffensen, J., Dahl-Jensen, D., Vinther, B. M., and Clausen, H. B.: The Greenland Ice Core Chronology 2005, 15–42 ka. Part 1: constructing the time scale, Quaternary Science Reviews, 25, 3246–3257, https://doi.org/10.1016/j.quascirev.2006.08.002, 2006.

Anvari, M., Tabar, M. R. R., Peinke, J., and Lehnertz, K.: Disentangling the stochastic behavior of complex time series, Scientific Reports, 6, 35 435, https://doi.org/10.1038/srep35435, 2016.

Applebaum, D.: Lévy Processes and Stochastic Calculus, Cambridge University Press, 2 edn., https://doi.org/10.1017/CBO9780511809781, 2011.

Armstrong McKay, D. I., Staal, A., Abrams, J. F., Winkelmann, R., Sakschewski, B., Loriani, S., Fetzer, I., Cornell, S. E., Rockström, J., and Lenton, T. M.: Exceeding 1.5°C global warming could trigger multiple climate tipping points, Science (New York, N.Y.), 377, eabn7950, https://doi.org/10.1126/science.abn7950, 2022.

Ashwin, P., Wieczorek, S., Vitolo, R., and Cox, P.: Tipping points in open systems: Bifurcation, noise-induced and rate-dependent examples in the climate system, Philosophical Transactions of the Royal Society A: Mathematical, Physical and Engineering Sciences, 370, 1166–1184, https://doi.org/10.1098/rsta.2011.0306, 2012.

Boers, N.: Early-warning signals for Dansgaard–Oeschger events in a high-resolution ice core record, Nature Communications, 9, 2556, https://doi.org/10.1038/s41467-018-04881-7, 2018.

Boers, N.: Observation-based early-warning signals for a collapse of the Atlantic Meridional Overturning Circulation, Nature Climate Change, 11, 680–688, https://doi.org/10.1038/s41558-021-01097-4, 2021.

Boers, N. and Rypdal, M.: Critical slowing down suggests that the western Greenland Ice Sheet is close to a tipping point, Proceedings of the National Academy of Sciences, 118, e2024192 118, https://doi.org/10.1073/pnas.2024192118, 2021.

Boers, N., Chekroun, M. D., Liu, H., Kondrashov, D., Rousseau, D.-D., Svensson, A., Bigler, M., and Ghil, M.: Inverse stochastic–dynamic models for high-resolution Greenland ice core records, Earth System Dynamics, 8, 1171–1190, https://doi.org/10.5194/esd-8-1171-2017, 2017.

Boers, N., Ghil, M., and Rousseau, D. D.: Ocean circulation, ice shelf, and sea ice interactions explain Dansgaard–Oeschger cycles, Proceedings of the National Academy of Sciences of the United States of America, 115, E11 005–E11 014, https://doi.org/10.1073/pnas.1802573115, 2018.

Boers, N., Lenton, T., and Rypdal, M.: Observational evidence for the destabilization of five Earth system tipping elements, under review, 2021.

Boers, N., Ghil, M., and Stocker, T. F.: Theoretical and paleoclimatic evidence for abrupt transitions in the Earth system, Environmental Research Letters, 17, 093 006, https://doi.org/10.1088/1748-9326/ac8944, 2022.

Boulton, C. A., Allison, L. C., and Lenton, T. M.: Early warning signals of Atlantic Meridional Overturning Circulation collapse in a fully coupled climate model, Nature Communications, 5, 5752, https://doi.org/10.1038/ncomms6752, 2014.

Boulton, C. A., Lenton, T. M., and Boers, N.: Pronounced loss of Amazon rainforest resilience since the early 2000s, Nature Climate Change, 12, 271–278, https://doi.org/10.1038/s41558-022-01287-8, 2022.

Broecker, W. S., Peteet, D. M., and Rind, D.: Does the ocean-atmosphere system have more than one stable mode of operation?, Nature, 315, 21–26, https://doi.org/10.1038/315021a0, 1985.

Brovkin, V., Brook, E., Williams, J. W., Bathiany, S., Lenton, T. M., Barton, M., DeConto, R. M., Donges, J. F., Ganopolski, A., McManus, J., Praetorius, S., de Vernal, A., Abe-Ouchi, A., Cheng, H., Claussen, M., Crucifix, M., Gallopín, G., Iglesias, V., Kaufman, D. S., Kleinen, T., Lambert, F., van der Leeuw, S., Liddy, H., Loutre, M.-f., McGee, D., Rehfeld, K., Rhodes, R., Seddon, A. W. R., Trauth, M. H., Vanderveken, L., and Yu, Z.: Past abrupt changes, tipping points and cascading impacts in the Earth system, Nature Geoscience, 14, 550–558, https://doi.org/10.1038/s41561-021-00790-5, 2021.

Capron, E., Rasmussen, S. O., Popp, T. J., Erhardt, T., Fischer, H., Landais, A., Pedro, J. B., Vettoretti, G., Grinsted, A., Gkinis, V., Vaughn, B., Svensson, A., Vinther, B. M., and White, J. W.: The anatomy of past abrupt warmings recorded in Greenland ice, Nature Communications, 12, 2106, https://doi.org/10.1038/s41467-021-22241-w, 2021.

Chechkin, A. V., Klafter, J., Gonchar, V. Y., Metzler, R., and Tanatarov, L. V.: Bifurcation, bimodality, and finite variance in confined Lévy flights, Physical Review E, 67, 010 102, https://doi.org/10.1103/PhysRevE.67.010102, 2003.

Chechkin, A. V., Gonchar, V. Y., Klafter, J., Metzler, R., and Tanatarov, L. V.: Lévy Flights in a Steep Potential Well, Journal of Statistical Physics, 115, 1505–1535, https://doi.org/10.1023/B:JOSS.0000028067.63365.04, 2004.

Cheng, H., Sinha, A., Cruz, F. W., Wang, X., Edwards, R. L., D'Horta, F. M., Ribas, C. C., Vuille, M., Stott, L. D., and Auler, A. S.: Climate change patterns in Amazonia and biodiversity, Nature Communications, 4, 1411, https://doi.org/10.1038/ncomms2415, 2013.

Cimatoribus, A. A., Drijfhout, S. S., Livina, V., and Van Der Schrier, G.: Dansgaard–Oeschger events: Bifurcation points in the climate system, Climate of the Past, 9, 323–333, https://doi.org/10.5194/cp-9-323-2013, 2013.

Clark, P. U., Pisias, N. G., Stocker, T. F., and Weaver, A. J.: The role of the thermohaline circulation in abrupt climate change, Nature, 415, 863–869, https://doi.org/10.1038/415863a, 2002.

Corrick, E. C., Drysdale, R. N., Hellstrom, J. C., Capron, E., Rasmussen, S. O., Zhang, X., Fleitmann, D., Couchoud, I., Wolff, E., and Monsoon, S. A.: Synchronous timing of abrupt climate changes during the last glacial period, Science, 369, 963–969, https://doi.org/10.1126/science.aay5538, 2020.

Dansgaard, W., Clausen, H. B., Gundestrup, N., Hammer, C. U., Johnsen, S. F., Kristinsdottir, P. M., and Reeh, N.: A New Greenland Deep Ice Core, Science, 218, 1273–1278, https://doi.org/10.1126/science.218.4579.1273, 1982.

Dansgaard, W., Johnsen, S., Clausen, H., Dahl-Jensen, D., Gundestrup, N., Hammer, C., and Oeschger, H.: North Atlantic Climatic Oscillations Revealed by Deep Greenland Ice Cores, pp. 288–298, American Geophysical Union, https://doi.org/10.1029/GM029p0288, 1984.

Dansgaard, W., Johnsen, S. J., Clausen, H. B., Dahl-Jensen, D., Gundestrup, N. S., Hammer, C. U., Hvidberg, C. S., Steffensen, J. P., Sveinbjörnsdottir, A. E., Jouzel, J., and Bond, G.: Evidence for general instability of past climate from a 250-kyr ice-core record, Nature, 364, 218–220, https://doi.org/10.1038/364218a0, 1993.

Davis, W. and Buffett, B.: Estimation of drift and diffusion functions from unevenly sampled time-series data, Physical Review E, 106, 014 140, https://doi.org/10.1103/PhysRevE.106.014140, 2022.

Ditlevsen, P. D.: Observation of α-stable noise induced millennial climate changes from an ice-core record, Geophysical Research Letters, 26, 1441–1444, https://doi.org/10.1029/1999GL900252, 1999.

Ditlevsen, P. D., Andersen, K. K., and Svensson, A.: The DO-climate events are probably noise induced: statistical investigation of the claimed 1470 years cycle, Climate of the Past, 3, 129–134, https://doi.org/10.5194/cp-3-129-2007, 2007.

Dokken, T. M., Nisancioglu, K. H., Li, C., Battisti, D. S., and Kissel, C.: Dansgaard–Oeschger cycles: Interactions between ocean and sea ice intrinsic to the Nordic seas, Paleoceanography, 28, 491–502, https://doi.org/10.1002/palo.20042, 2013.

Einstein, A.: Über die von der molekularkinetischen Theorie der Wärme geforderte Bewegung von in ruhenden Flüssigkeiten suspendierten Teilchen, Annalen der Physik, 322, 549–560, https://doi.org/10.1002/andp.19053220806, 1905.

Epanechnikov, V. A.: Non-Parametric Estimation of a Multivariate Probability Density, Theory of Probability & Its Applications, 14, 153–158, https://doi.org/10.1137/1114019, 1967.

EPICA Community Members: One-to-one coupling of glacial climate variability in Greenland and Antarctica, Nature, 444, 5–8, https://doi.org/doi:10.1038/nature05301, 2006.

Erhardt, T., Capron, E., Olander Rasmussen, S., Schüpbach, S., Bigler, M., Adolphi, F., and Fischer, H.: Decadal-scale progression of the onset of Dansgaard–Oeschger warming events, Climate of the Past, 15, 811–825, https://doi.org/10.5194/cp-15-811-2019, 2019.

Fischer, H., Siggaard-Andersen, M. L., Ruth, U., Röthlisberger, R., and Wolff, E.: Glacial/interglacial changes in mineral dust and sea-salt records in polar ice cores: Sources, transport, and deposition, Reviews of Geophysics, 45, 1–26, https://doi.org/10.1029/2005RG000192, 2007.

Fokker, A. D.: Over Brown'sche bewegingen in het stralingsveld, en waarschijnlijkheids-beschouwingen in de stralingstheorie, Ph.D. thesis, University of Leiden, http://ilorentz.org/history/proefschriften/sources/Fokker_1913.pdf, 1913.

Fokker, A. D.: Die mittlere Energie rotierender elektrischer Dipole im Strahlungsfeld, Annalen der Physik, 348, 810–820, https://doi.org/10.1002/andp.19143480507, 1914.

Friedrich, R., Peinke, J., Sahimi, M., and Tabar, M. R. R.: Approaching complexity by stochastic methods: From biological systems to turbulence, Physics Reports, 506, 87–162, https://doi.org/10.1016/j.physrep.2011.05.003, 2011.

Fuhrer, K., Neftel, A., Anklin, M., and Maggi, V.: Continuous measurements of hydrogen peroxide, formaldehyde, calcium and ammonium concentrations along the new grip ice core from summit, Central Greenland, Atmospheric Environment Part A, General Topics, 27, 1873–1880, https://doi.org/10.1016/0960-1686(93)90292-7, 1993.

Fuhrer, K., Wolff, E. W., and Johnsen, S. J.: Timescales for dust variability in the Greenland Ice Core Project (GRIP) ice core in the last 100,000 years, Journal of Geophysical Research Atmospheres, 104, 31 043–31 052, https://doi.org/10.1029/1999JD900929, 1999.

Ganopolski, A. and Rahmstorf, S.: Rapid changes of glacial climate simulated in a coupled climate model, Nature, 409, 153–158, https://doi.org/10.1038/35051500, 2001.

Ganopolski, A. and Rahmstorf, S.: Abrupt Glacial Climate Changes due to Stochastic Resonance, Physical Review Letters, 88, 4, https://doi.org/10.1103/PhysRevLett.88.038501, 2002.

Gardiner, C.: Stochastic Methods: A Handbook for the Natural and Social Sciences, Springer-Verlag Berlin Heidelberg, 4 edn., 2009.

Ghil, M.: Steady-State Solutions of a Diffusive Energy-Balance Climate Model and Their Stability, Tech. Rep. IMM410, Courant Institute of Mathematical Sciences, New York University, New York, https://ntrs.nasa.gov/api/citations/19750014903/downloads/19750014903.pdf, 1975.

Gkinis, V., Simonsen, S. B., Buchardt, S. L., White, J. W., and Vinther, B. M.: Water isotope diffusion rates from the NorthGRIP ice core for the last 16,000 years – Glaciological and paleoclimatic implications, Earth and Planetary Science Letters, 405, 132–141, https://doi.org/10.1016/j.epsl.2014.08.022, 2014.

Gottschalk, J., Skinner, L. C., Misra, S., Waelbroeck, C., Menviel, L., and Timmermann, A.: Abrupt changes in the southern extent of North Atlantic Deep Water during Dansgaard-Oeschger events, Nature Geoscience, 8, 950–954, https://doi.org/10.1038/ngeo2558, 2015.

Gottschall, J. and Peinke, J.: On the definition and handling of different drift and diffusion estimates, New Journal of Physics, 10, 083 034, https://doi.org/10.1088/1367-2630/10/8/083034, 2008.

Gottwald, G. A.: A model for Dansgaard–Oeschger events and millennial-scale abrupt climate change without external forcing, Climate Dynamics, 56, 227–243, https://doi.org/10.1007/s00382-020-05476-z, 2020.

Harris, C. R., Millman, K. J., van der Walt, S. J., Gommers, R., Virtanen, P., Cournapeau, D., Wieser, E., Taylor, J., Berg, S., Smith, N. J., Kern, R., Picus, M., Hoyer, S., van Kerkwijk, M. H., Brett, M., Haldane, A., Fernández del Río, J., Wiebe, M., Peterson, Pearu andGérard-Marchant, P., Sheppard, K., Reddy, T., Weckesser, W., Abbasi, H., Gohlke, C., and Oliphant, T. E.: Array programming with NumPy, Nature, 585, 357–362, https://doi.org/10.1038/s41586-020-2649-2, 2020.

Hassanibesheli, F., Boers, N., and Kurths, J.: Reconstructing complex system dynamics from time series: a method comparison, New Journal of Physics, 22, 073 053, https://doi.org/10.1088/1367-2630/ab9ce5, 2020.

Havlin, S. and Ben-Avraham, D.: Diffusion in disordered media, Advances in Physics, 36, 695–798, https://doi.org/10.1080/00018738700101072, 1987.

Heinze, C., Blenckner, T., Martins, H., Rusiecka, D., Döscher, R., Gehlen, M., Gruber, N., Holland, E., Hov, Ø., Joos, F., Matthews, J. B. R., Rødven, R., and Wilson, S.: The quiet crossing of ocean tipping points, Proceedings of the National Academy of Sciences of the United States of America, 118, 1–9, https://doi.org/10.1073/pnas.2008478118, 2021.

Henry, L. G., McManus, J. F., Curry, W. B., Roberts, N. L., Piotrowski, A. M., and Keigwin, L. D.: North Atlantic ocean circulation and abrupt climate change during the last glaciation, Science, 353, 470–474, https://doi.org/10.1126/science.aaf5529, 2016.

Hunter, J. D.: Matplotlib: A 2D Graphics Environment, Computing in Science Engineering, 9, 90–95, https://doi.org/10.1109/MCSE.2007.55, 2007.

J. P. Steffensen, Centre for Ice and Climate, Niels Bohr Institute: Data, icesamples and software, https://www.iceandclimate.nbi.ku.dk/data/, 2014.

Johnsen, S. J., Clausen, H. B., Dansgaard, W., Fuhrer, K., Gundestrup, N., Hammer, C. U., Iversen, P., Jouzel, J., Stauffer, B., and Steffensen, J.: Irregular glacial interstadials recorded in a new Greenland ice core, Nature, 359, 311–313, https://doi.org/10.1038/359311a0, 1992.

Johnsen, S. J., Dahl-Jensen, D., Gundestrup, N., Steffensen, J. P., Clausen, H. B., Miller, H., Masson-Delmotte, V., Sveinbjörnsdottir, A. E., and White, J.: Oxygen isotope and palaeotemperature records from six Greenland ice-core stations: Camp Century, Dye-3, GRIP, GISP2, Renland and NorthGRIP, Journal of Quaternary Science, 16, 299–307, https://doi.org/10.1002/jqs.622, 2001.

Jouzel, J., Alley, R. B., Cuffey, K. M., Dansgaard, W., Grootes, P., Hoffmann, G., Johnsen, S. J., Koster, R. D., Peel, D., Shuman, C. A., Stievenard, M., Stuiver, M., and White, J.: Validity of the temperature reconstruction from water isotopes in ice cores, Journal of Geophysical Research: Oceans, 102, 26 471–26 487, https://doi.org/10.1029/97JC01283, 1997.

Kanner, L. C., Burns, S. J., Cheng, H., and Edwards, R. L.: High-Latitude Forcing of the South American Summer Monsoon During the Last Glacial, Science, 335, 570–573, https://doi.org/10.1126/science.1213397, 2012.

Kindler, P., Guillevic, M., Baumgartner, M., Schwander, J., Landais, A., and Leuenberger, M.: Temperature reconstruction from 10 to 120 kyr b2k from the NGRIP ice core, Climate of the Past, 10, 887–902, https://doi.org/10.5194/cp-10-887-2014, 2014.

Kleppin, H., Jochum, M., Otto-Bliesner, B., Shields, C. A., and Yeager, S.: Stochastic atmospheric forcing as a cause of Greenland climate transitions, Journal of Climate, 28, 7741–7763, https://doi.org/10.1175/JCLI-D-14-00728.1, 2015.

Kondrashov, D., Kravtsov, S., Robertson, A. W., and Ghil, M.: A Hierarchy of Data-Based ENSO Models, Journal of Climate, 18, 4425–4444, https://doi.org/10.1175/JCLI3567.1, 2005.

Kondrashov, D., Chekroun, M. D., and Ghil, M.: Data-driven non-Markovian closure models, Physica D: Nonlinear Phenomena, 297, 33–55, https://doi.org/10.1016/j.physd.2014.12.005, 2015.

Kramers, H. A.: Brownian motion in a field of force and the diffusion model of chemical reactions, Physica, 7, 284–304, https://doi.org/10.1016/S0031-8914(40)90098-2, 1940.

Krumscheid, S., Pradas, M., Pavliotis, G. A., and Kalliadasis, S.: Data-driven coarse graining in action: Modeling and prediction of complex systems, Physical Review E, 92, 042 139, https://doi.org/10.1103/PhysRevE.92.042139, 2015.

Kwasniok, F.: Analysis and modelling of glacial climate transitions using simple dynamical systems, Philosophical Transactions of the Royal Society A: Mathematical, Physical and Engineering Sciences, 371, 20110 472, https://doi.org/10.1098/rsta.2011.0472, 2013.

Lamouroux, D. and Lehnertz, K.: Kernel-based regression of drift and diffusion coefficients of stochastic processes, Physics Letters A, 373, 3507–3512, https://doi.org/10.1016/j.physleta.2009.07.073, 2009.

Lehnertz, K., Zabawa, L., and Tabar, M. R. R.: Characterizing abrupt transitions in stochastic dynamics, New Journal of Physics, 20, 113 043, https://doi.org/10.1088/1367-2630/aaf0d7, 2018.

Lenton, T., Held, H., Kriegler, E., Hall, J. W., Lucht, W., Rahmstorf, S., and Schellnhuber, H. J.: Tipping elements in the Earth's climate system, Proceedings of the National Academy of Sciences of the United States of America, 105, 1786–1793, https://doi.org/10.1073/pnas.0705414105, 2008.

Lenton, T. M. and Schellnhuber, H. J.: Tipping the Scales, Nature Climate Change, 1, 97–98, https://doi.org/10.1038/climate.2007.65, 2007.

Li, C. and Born, A.: Coupled atmosphere-ice-ocean dynamics in Dansgaard–Oeschger events, Quaternary Science Reviews, 203, 1–20, https://doi.org/10.1016/j.quascirev.2018.10.031, 2019.

Li, C., Battisti, D. S., Schrag, D. P., and Tziperman, E.: Abrupt climate shifts in Greenland due to displacements of the sea ice edge, Geophysical Research Letters, 32, L19 702, https://doi.org/10.1029/2005GL023492, 2005.

Li, T.-Y., Han, L.-Y., Cheng, H., Edwards, R. L., Shen, C.-C., Li, H.-C., Li, J.-Y., Huang, C.-X., Zhang, T.-T., Zhao, X., and et al.: Evolution of the Asian summer monsoon during Dansgaard/Oeschger events 13–17 recorded in a stalagmite constrained by high-precision chronology from southwest China, Quaternary Research, 88, 121–128, https://doi.org/10.1017/qua.2017.22, 2017.

Lind, P. G., Mora, A., Gallas, J. A. C., and Haase, M.: Reducing stochasticity in the North Atlantic Oscillation index with coupled Langevin equations, Physical Review E, 72, 056 706, https://doi.org/10.1103/PhysRevE.72.056706, 2005.

Livina, V. N., Kwasniok, F., and Lenton, T. M.: Potential analysis reveals changing number of climate states during the last 60 kyr, Climate of the Past Discussions, 5, 2223–2237, https://doi.org/10.5194/cpd-5-2223-2009, 2010.

Lohmann, J. and Ditlevsen, P. D.: A consistent statistical model selection for abrupt glacial climate changes, Climate Dynamics, 52, 6411–6426, https://doi.org/10.1007/s00382-018-4519-2, 2018a.

Lohmann, J. and Ditlevsen, P. D.: Random and externally controlled occurrences of Dansgaard–Oeschger events, Climate of the Past, pp. 609–617, https://doi.org/10.5194/cp-14-609-2018, 2018b.

Lohmann, J., Castellana, D., Ditlevsen, P. D., and Dijkstra, H. A.: Abrupt climate change as a rate-dependent cascading tipping point, Earth System Dynamics, 12, 819–835, https://doi.org/10.5194/esd-12-819-2021, 2021.

Lynch-Stieglitz, J.: The Atlantic Meridional Overturning Circulation and Abrupt Climate Change, Annual Review of Marine Science, 9, 83–104, https://doi.org/10.1146/annurev-marine-010816-060415, 2017.

Menviel, L. C., Skinner, L. C., Tarasov, L., and Tzedakis, P. C.: An ice–climate oscillatory framework for Dansgaard–Oeschger cycles, Nature Reviews Earth & Environment, 1, 677–693, https://doi.org/10.1038/s43017-020-00106-y, 2020.

Metzler, R. and Klafter, J.: The restaurant at the end of the random walk: recent developments in the description of anomalous transport by fractional dynamics, Journal of Physics A: Mathematical and General, 37, R161–R208, https://doi.org/10.1088/0305-4470/37/31/r01, 2004.

Mitsui, T. and Crucifix, M.: Influence of external forcings on abrupt millennial-scale climate changes: a statistical modelling study, Climate Dynamics, 48, 2729–2749, https://doi.org/10.1007/s00382-016-3235-z, 2017.

Moyal, J. E.: Stochastic processes and statistical physics, J. R. Stat. Soc. Series B (Methodological), 11, 150–210, http://www.jstor.org/stable/2984076, 1949.

Nadaraya, E. A.: On Estimating Regression, Theory of Probability & Its Applications, 9, 141–142, https://doi.org/10.1137/1109020, 1964.

North, G. R.: Analytical Solution to a Simple Climate Model with Diffusive Heat Transport, Journal of the Atmospheric Sciences, 32, 1301–1307, https://doi.org/10.1175/1520-0469(1975)032<1301:ASTASC>2.0.CO;2, 1975.

North Greenland Ice Core Projects members: High-resolution record of Northern Hemisphere climate extending into the last interglacial period, Nature, 431, 147–151, https://doi.org/10.1038/nature02805, 2004.

Pawula, R. F.: Generalizations and extensions of the Fokker–Planck–Kolmogorov equations, IEEE Transactions on Information Theory, 13, 33–41, https://doi.org/10.1109/TIT.1967.1053955, 1967a.

Pawula, R. F.: Approximation of the Linear Boltzmann Equation by the Fokker–Planck Equation, Physical Review, 162, 186–188, https://doi.org/10.1103/PhysRev.162.186, 1967b.

Petersen, S. V., Schrag, D. P., and Clark, P. U.: A new mechanism for Dansgaard–Oeschger cycles, Paleoceanography, 28, 24–30, https://doi.org/10.1029/2012PA002364, 2013.

Planck, M.: Sitzber. Preuß. Akad. Wiss. p. 324, 1917.

Rasmussen, S. O., Andersen, K. K., Svensson, A. M., Steffensen, J. P., Vinther, B. M., Clausen, H. B., Siggaard-Andersen, M. L., Johnsen, S. J., Larsen, L. B., Dahl-Jensen, D., Bigler, M., Röthlisberger, R., Fischer, H., Goto-Azuma, K., Hansson, M. E., and Ruth, U.: A new Greenland ice core chronology for the last glacial termination, Journal of Geophysical Research Atmospheres, 111, D06 102, https://doi.org/10.1029/2005JD006079, 2006.

Rasmussen, S. O., Bigler, M., Blockley, S. P., Blunier, T., Buchardt, S. L., Clausen, H. B., Cvijanovic, I., Dahl-Jensen, D., Johnsen, S. J., Fischer, H., Gkinis, V., Guillevic, M., Hoek, W. Z., Lowe, J. J., Pedro, J. B., Popp, T., Seierstad, I. K., Steffensen, J. P., Svensson, A. M., Vallelonga, P., Vinther, B. M., Walker, M. J., Wheatley, J. J., and Winstrup, M.: A stratigraphic framework for abrupt climatic changes during the Last Glacial period based on three synchronized Greenland ice-core records: Refining and extending the INTIMATE event stratigraphy, Quaternary Science Reviews, 106, 14–28, https://doi.org/10.1016/j.quascirev.2014.09.007, 2014.

Rial, J. A. and Saha, R.: Modeling Abrupt Climate Change as the Interaction Between Sea Ice Extent and Mean Ocean Temperature Under Orbital Insolation Forcing, pp. 57–74, American Geophysical Union (AGU), https://doi.org/10.1029/2010GM001027, 2011.

Risken, H. and Frank, T.: The Fokker–Planck equation, Springer-Verlag, Berlin, Heidelberg, 2 edn., https://doi.org/10.1007/978-3-642-61544-3, 1996.

Roberts, A. and Saha, R.: Relaxation oscillations in an idealized ocean circulation model, Climate Dynamics, 48, 2123–2134, https://doi.org/10.1007/s00382-016-3195-3, 2017.

Rosier, S. H., Reese, R., Donges, J. F., De Rydt, J., Hilmar Gudmundsson, G., and Winkelmann, R.: The tipping points and early warning indicators for Pine Island Glacier, West Antarctica, Cryosphere, 15, 1501–1516, https://doi.org/10.5194/tc-15-1501-2021, 2021.

Ruth, U., Wagenbach, D., Steffensen, J. P., and Bigler, M.: Continuous record of microparticle concentration and size distribution in the central Greenland NGRIP ice core during the last glacial period, Journal of Geophysical Research: Atmospheres, 108, 4098, https://doi.org/10.1029/2002JD002376, 2003.

Ruth, U., Bigler, M., Röthlisberger, R., Siggaard-Andersen, M. L., Kipfstuhl, S., Goto-Azuma, K., Hansson, M. E., Johnsen, S. J., Lu, H., and Steffensen, J. P.: Ice core evidence for a very tight link between North Atlantic and east Asian glacial climate, Geophysical Research Letters, 34, L03 706, https://doi.org/10.1029/2006GL027876, 2007.

Rydin Gorjão, L. and Meirinhos, F.: `kramersmoyal`: Kramers–Moyal coefficients for stochastic processes, Journal of Open Source Software, 4, 1693, https://doi.org/10.21105/joss.01693, 2019.

Rydin Gorjão, L., Heysel, J., Lehnertz, K., and Tabar, M. R. R.: Analysis and data-driven reconstruction of bivariate jump-diffusion processes, Physical Review E, 100, 062 127, https://doi.org/10.1103/PhysRevE.100.062127, 2019.

Rydin Gorjão, L., Witthaut, D., Lehnertz, K., and Lind, P. G.: Arbitrary-Order Finite-Time Corrections for the Kramers–Moyal Operator, Entropy, 23, 517, https://doi.org/10.3390/e23050517, 2021.

Schüpbach, S., Fischer, H., Bigler, M., Erhardt, T., Gfeller, G., Leuenberger, D., Mini, O., Mulvaney, R., Abram, N. J., Fleet, L., Frey, M. M., Thomas, E., Svensson, A., Dahl-Jensen, D., Kettner, E., Kjaer, H., Seierstad, I., Steffensen, J. P., Rasmussen, S. O., Vallelonga, P., Winstrup, M., Wegner, A., Twarloh, B., Wolff, K., Schmidt, K., Goto-Azuma, K., Kuramoto, T., Hirabayashi, M., Uetake, J., Zheng, J., Bourgeois, J., Fisher, D., Zhiheng, D., Xiao, C., Legrand, M., Spolaor, A., Gabrieli, J., Barbante, C., Kang, J. H., Hur, S. D., Hong, S. B., Hwang, H. J., Hong, S., Hansson, M., Iizuka, Y., Oyabu, I., Muscheler, R., Adolphi, F., Maselli, O., McConnell, J., and Wolff, E. W.: Greenland records of aerosol source and atmospheric lifetime changes from the Eemian to the Holocene, Nature Communications, 9, 1476, https://doi.org/10.1038/s41467-018-03924-3, 2018.

Seierstad, I. K., Abbott, P. M., Bigler, M., Blunier, T., Bourne, A. J., Brook, E., Buchardt, S. L., Buizert, C., Clausen, H. B., Cook, E., Dahl-Jensen, D., Davies, S. M., Guillevic, M., Johnsen, S. J., Pedersen, D. S., Popp, T. J., Rasmussen, S. O., Severinghaus, J. P., Svensson, A., and Vinther, B. M.: Consistently dated records from the Greenland GRIP, GISP2 and NGRIP ice cores for the past 104 ka reveal regional millennial-scale $\delta^{18}O$ gradients with possible Heinrich event imprint, Quaternary Science Reviews, 106, 29–46, https://doi.org/0.1016/j.quascirev.2014.10.032, 2014.

Silverman, B. W.: Density Estimation for Statistics and Data Analysis, Routledge, Boca Raton, 1st edition edn., https://doi.org/10.1201/9781315140919, 1998.

Snyder, C. W.: Evolution of global temperature over the past two million years, Nature, 538, 226–228, https://doi.org/10.1038/nature19798, 2016.

Steffensen, J. P., Andersen, K. K., Bigler, M., Clausen, H. B., Dahl-jensen, D., Fischer, H., Goto-azuma, K., Hansson, M., Johnsen, S. J., Jouzel, J., Masson-delmotte, V., Popp, T., Rasmussen, S. O., Röthlisberger, R., Ruth, U., Stauffer, B., Sveinbjörnsdóttir, Á. E., Svensson, A., and White, J. W. C.: High-Resolution Greenland Ice Core Data Show Abrupt Climate Change Happens in Few Years, Science, 321, 680–684, https://doi.org/10.1126/science.1157707, 2008.

Stemler, T., Werner, J. P., Benner, H., and Just, W.: Stochastic Modeling of Experimental Chaotic Time Series, Physical Review Letters, 98, 044 102, https://doi.org/10.1103/PhysRevLett.98.044102, 2007.

Stommel, H.: Thermohahe Convection with Two Stable Regimes, Tellus, 13, 224–230, 1961.

Svensson, A., Andersen, K. K., Bigler, M., Clausen, H. B., Dahl-Jensen, D., Johnsen, S. J., Rasmussen, S. O., Seierstad, I., Steffensen, J. P., Svensson, A., Vinther, B. M., Davies, S. M., Muscheler, R., Parrenin, F., and Röthlisberger, R.: A 60 000 year Greenland stratigraphic ice core chronology, Climate of the Past Discussions, 3, 1235–1260, https://doi.org/10.5194/cpd-3-1235-2007, 2008.

Tabar, M. R. R.: Analysis and Data-Based Reconstruction of Complex Nonlinear Dynamical Systems, Springer International Publishing, https://doi.org/10.1007/978-3-030-18472-8, 2019.

Valdes, P.: Built for stability, Nature Geoscience, 4, 414–416, https://doi.org/10.1038/ngeo1200, 2011.

van Kampen, N. G.: A power series expansion of the master equation, Canadian Journal of Physics, 39, 551–567, https://doi.org/10.1139/p61-056, 1961.

Vettoretti, G. and Peltier, W. R.: Fast physics and slow physics in the nonlinear Dansgaard–Oeschger relaxation oscillation, Journal of Climate, 31, 3423–3449, https://doi.org/10.1175/JCLI-D-17-0559.1, 2018.

Vettoretti, G., Ditlevsen, P., Jochum, M., and Rasmussen, S. O.: Atmospheric CO2 control of spontaneous millennial-scale ice age climate oscillations, Nature Geoscience, 15, 300–306, https://doi.org/10.1038/s41561-022-00920-7, 2022.

Vinther, B. M., Clausen, H. B., Johnsen, S. J., Rasmussen, S. O., Andersen, K. K., Buchardt, S. L., Dahl-Jensen, D., Seierstad, I. K., Siggaard-Andersen, M. L., Steffensen, J. P., Svensson, A., Olsen, J., and Heinemeier, J.: A synchronized dating of three Greenland ice cores throughout the Holocene, Journal of Geophysical Research Atmospheres, 111, D13 102, https://doi.org/10.1029/2005JD006921, 2006.

Virtanen, P., Gommers, R., Oliphant, T. E., Haberland, M., Reddy, T., Cournapeau, D., Burovski, E., Peterson, P., Weckesser, W., Bright, J., van der Walt, S. J., Brett, M., Wilson, J., Millman, K. J., Mayorov, N., Nelson, A. R. J., Jones, E., Kern, R., Larson, E., Carey, C. J., Polat, İ., Feng, Y., Moore, E. W., VanderPlas, J., Laxalde, D., Perktold, J., Cimrman, R., Henriksen, I., Quintero, E. A., Harris, C. R., Archibald, A. M., Ribeiro, A. H., Pedregosa, F., van Mulbregt, P., and SciPy 1.0 Contributors: SciPy 1.0: Fundamental Algorithms for Scientific Computing in Python, Nature Methods, 17, 261–272, https://doi.org/10.1038/s41592-019-0686-2, 2020.

Voelker, A. H.: Global distribution of centennial-scale records for Marine Isotope Stage (MIS) 3: A database, Quaternary Science Reviews, 21, 1185–1212, https://doi.org/10.1016/S0277-3791(01)00139-1, 2002.

von Smoluchowski, M.: Zur kinetischen Theorie der Brownschen Molekularbewegung und der Suspensionen, Annalen der Physik, 326, 756–780, https://doi.org/10.1002/andp.19063261405, 1906.

WAIS Divide Project Members: Precise interpolar phasing of abrupt climate change during the last ice age, Nature, 520, 661–665, https://doi.org/10.1038/nature14401, 2015.

Wang, Y. J., Cheng, H., Edwards, R. L., An, Z. S., Wu, J. Y., Shen, C. C., and Dorale, J. A.: A high-resolution absolute-dated late pleistocene monsoon record from Hulu Cave, China, Science, 294, 2345–2348, https://doi.org/10.1126/science.1064618, 2001.

Watson, G. S.: Smooth Regression Analysis, Sankhyā: The Indian Journal of Statistics, Series A, 26, 359–372, http://www.jstor.org/stable/25049340, 1964.

Wes McKinney: Data Structures for Statistical Computing in Python, in: Proceedings of the 9th Python in Science Conference, edited by Stéfan van der Walt and Jarrod Millman, pp. 56–61, https://doi.org/10.25080/Majora-92bf1922-00a, 2010.

Woollings, T., Hannachi, A., and Hoskins, B.: Variability of the North Atlantic eddy-driven jet stream, Quarterly Journal of the Royal Meteorological Society, 136, 856–868, https://doi.org/10.1002/qj.625, 2010.

Zhang, X., Lohmann, G., Knorr, G., and Purcell, C.: Abrupt glacial climate shifts controlled by ice sheet changes, Nature, 512, 290–294, https://doi.org/10.1038/nature13592, 2014.

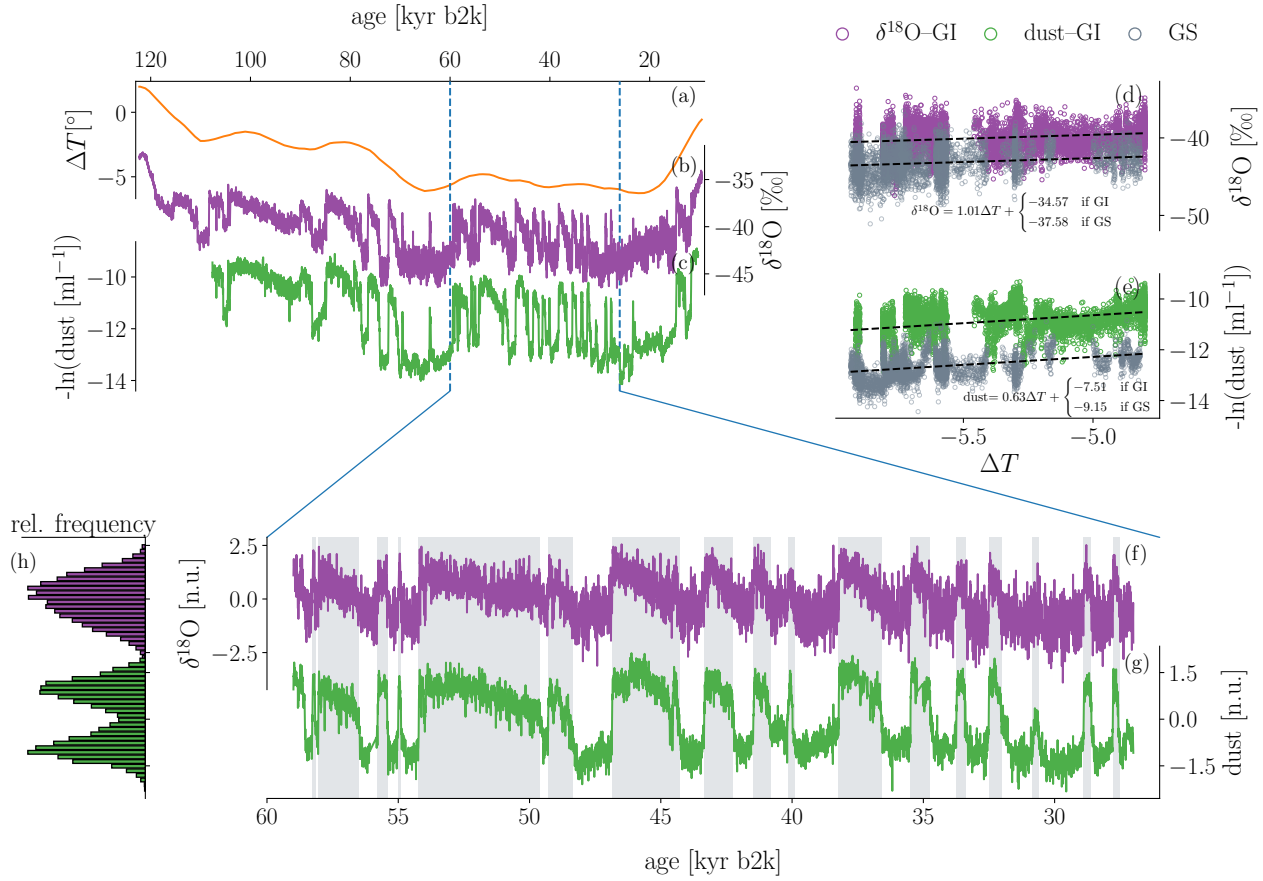

Figure 1. ~~The dust~~ (a) Global mean surface temperature reconstruction for the last glacial interval as provided by (Snyder, 2016) and linearly interpolated to a 20-year temporal resolution. The reconstruction is based on a multi-proxy database which comprises over 20 000 sea surface temperature reconstructions from 59 marine sediment cores. Shown is the anomaly with respect to modern climate (5–0 kyr b2k average, b2k=before 2000 CE). 20-year mean of δ^{18}O ratios (b) ~~records~~ and accordingly resampled dust concentrations (c) from the NGRIP ice core in Greenland, from ~~59~~ 122 kyr and 107 kyr to ~~27~~ 10 kyr~~before the year 2000 B.C.E. (~~b2k ~~)~~(Rasmussen et al., 2014; Seierstad et al., 2014; Ruth et al., 2003). The dust data is given as the negative natural logarithm of the actual dust concentrations, in order to facilitate visual comparison to the δ^{18}O data. ~~All time series are normalised~~Panels (d) and (e) show the linear regressions of δ^{18}O and dust onto the reconstructed global mean surface temperatures (Snyder, 2016) from (a), carried out separately for Greenland stadials (GS) and Greenland interstadials (GI). Panels (f) and (g) show the same proxies as shown in (b) and (c) but at a higher resolution of 5 yr (North Greenland Ice Core Projects members, 2004; Gkinis et al., 2014; Ruth et al., 2003) and over the shorter period from 59 to 27 kyr b2k. The analysis presented in this study was constrained to this section of the record. The two ~~proxies~~ proxy time series in (f) and (g) have been ~~pre-processed, in order to ensure stationarity,~~ detrended by removing ~~a linear trend drawn from~~ the slow nonlinear change induced by changes in the global ~~average surface~~ background temperatures, based on the regressions from (~~see App. ??~~d) and (e). The data were then binned to equidistant time resolution from the original 5 cm depth resolution. The grey shadings mark the Greenland ~~Interstadial~~ interstadial (GI) intervals according to (Rasmussen et al., 2014). ~~The~~ Panel (h) shows the histograms of the two time series ~~can be found~~ shown in (f) and (g), respectively. All data are shown on the GICC05 chronology ~~(J. P. Steffensen, Centre for Ice and Climate, Niels Bohr Institute, 2014; Seierstad et al., 2014)~~ (Vinther et al., 2006; Rasmussen et al., 2006; Andersen et al., 2006; Svensson et al., 2008).

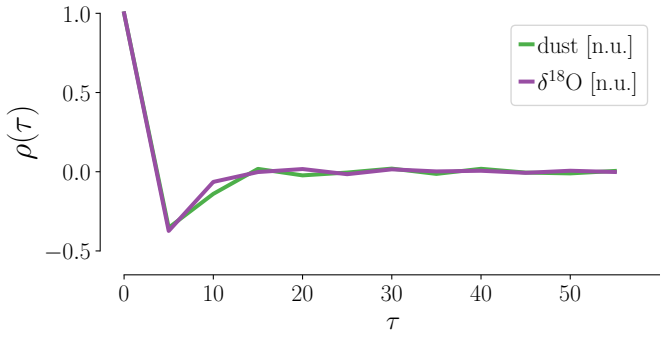

Figure 2. Autocorrelation $\rho(\tau)$ of the increments Δx_t of δ^{18}O and dust records. Both records show a weak anti-correlation at the shortest lag $\tau = 5y$, and no correlation for $\tau > 5y$. We thus consider the data Markovian.

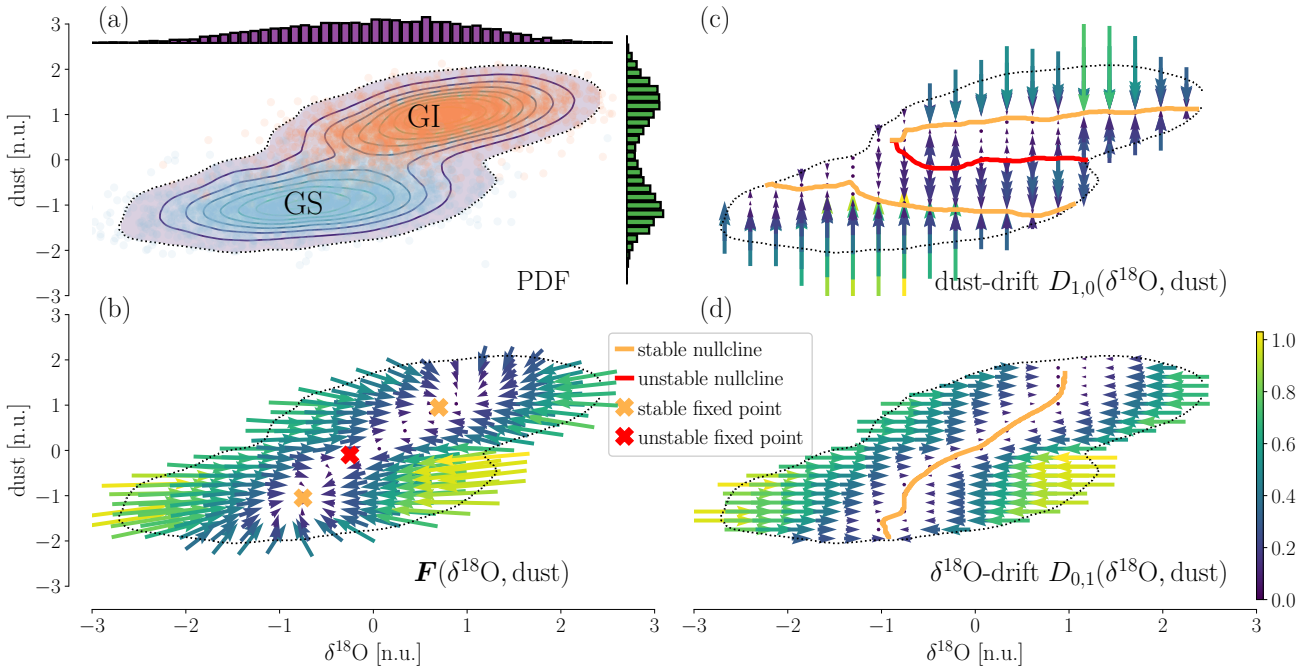

Figure 3. Two-dimensional drift reconstruction. (a) PDF of the two-dimensional record, with projections onto both dimensions. Blue and orange dots represent the individual data points from Greenland stadials (GS) and Greenland interstadials (GI), respectively. Contour lines are obtained from a kernel density estimate of the data distribution. The dotted contour line indicates a chosen cutoff data density of > 0.015 data points per pixel – regions in the state space with lower data density are not considered in the analysis. One pixel has the size of 0.015×0.015 in normalised units. (b) The reconstructed vector field $\boldsymbol{F}$ according to Eq. (5). Regions of convergence are apparent, which correspond to the GI and GS states of the record. (c) The dust component $D_{0,1}$ of the reconstructed drift. The dust's nullcline exhibits an *s*-shape two stable branches (orange) and an unstable one in between (red), indicative of a double-fold bifurcation with δ^{18}O as control parameter. (d) the δ^{18}O component $D_{1,0}$ of the reconstructed drift. Here, the nullcline is comprised of a single stable branch (orange). The position of δ^{18}O fixed point varies with the value of the dust. Fixed points of the coupled system are given by the intersections of the two component's nullclines, marked with an X in panel (b).

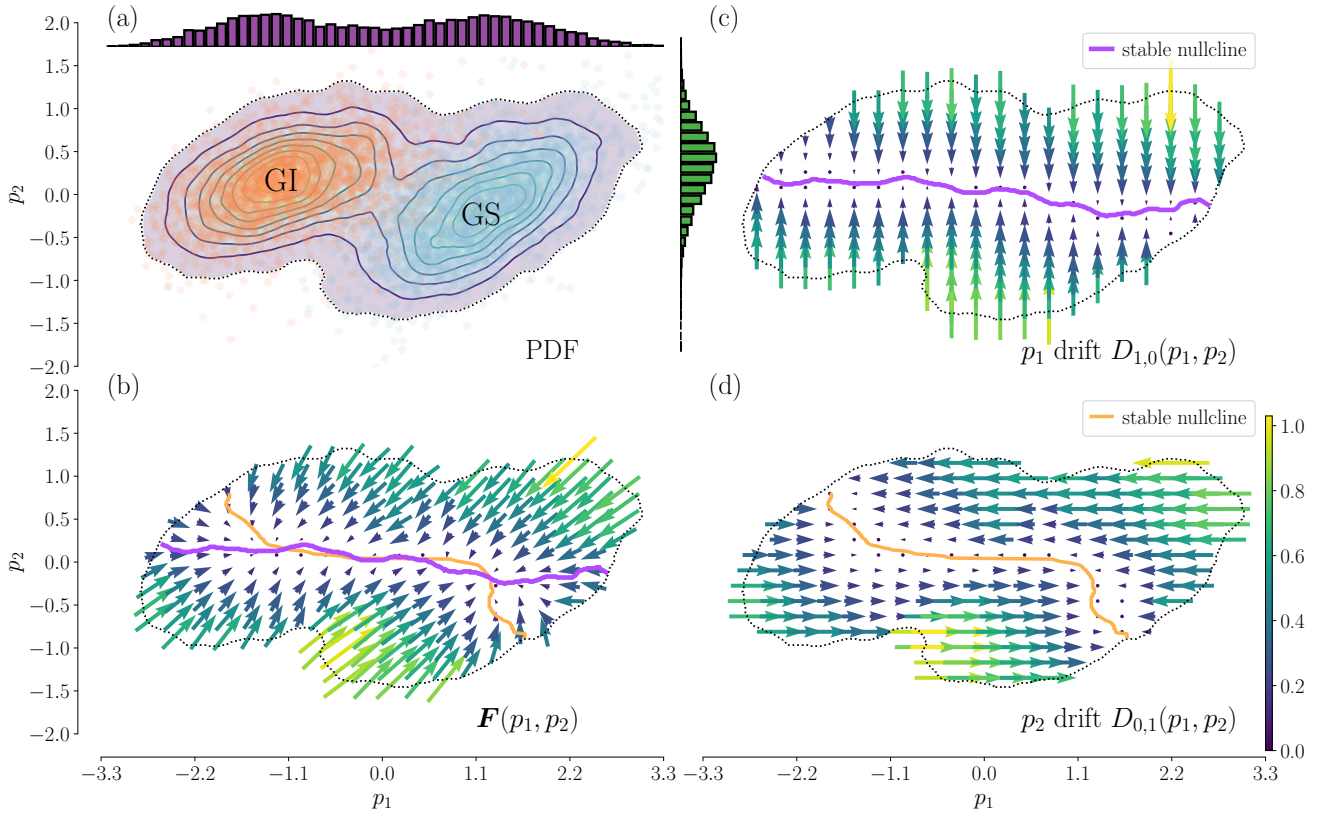

Figure 4. Redrawing of Fig. 3 in a rotated state space. The variables p_1 and p_2 represent the rotated time series, onto which the same KM analysis is performed as before. We can observe that even in this rotated setting we cannot disregard the coupling of the two variables. The doubled-fold structure is occluded by the rotation (see drift of the variable p_1, panel (c)). The drift of p_2 remains dependent on p_1 (see panel (d)). We can thus conclude that the observed coupling is not an artefact of the initial state space used and is an intrinsic characteristic of the two proxies.